

**Azothiazole probe as multianalyte colorimetric chemosensor for urea and biologically
significant amines**

Sapna Singh, Archana Velloth, Rishi Ram Mahato, Surbhi Grewal, Subhabrata Maiti* Sugumar

Venkataramani*

Department of Chemical Sciences, Indian Institute of Science Education and Research (IISER) Mohali,

Sector 81, SAS Nagar, Knowledge City, Manauli-140306, Punjab, India

E-mail: smaiti@iisermohali.ac.in, sugumarv@iisermohali.ac.in

Contents

| | |
|---|---------|
| S1. General methods | S2-S3 |
| S2. Spectroscopic studies | S4-S6 |
| S3. Quantitative analysis | S7-S9 |
| S4. Mechanism of sensing | S10-S12 |
| S5. Scope of detection and studies in gel | S13-S15 |
| S6. Long-term stability, reusability and pH stability of probe | S16-S17 |
| S7. Computational studies | S18-S26 |
| S8. Spectral characterization data (^1H , ^{13}C NMR data) | S27-S30 |
| S9. Other supporting information | S31 |
| S10. References | S32 |

S1. General methods:

Reagents and solvents: Starting materials for the probe synthesis, urea, urease, agarose powder, urine sample, blood serum, amino acids and other analytes used in the studies were obtained from commercial suppliers. All the solvents were purchased from commercially available sources such as Sigma Aldrich, Avra, Rankem, Spectrochem, TCI, etc., and used without further purification. HPLC or spectroscopic grade solvents have been used for UV-vis studies and NMR studies. For column chromatography, pre-distilled solvents have been utilized. Mili-Q water and phosphate buffer was used for UV-Vis and gelation studies.

Chromatography: Thin layer chromatography was performed on Merck Silica gel 60 F₂₅₄ TLC plates, and visualized using a UV chamber ($\lambda = 254$ nm). Column chromatography was performed over (100-200 mesh) silica gel.

NMR spectroscopy: ¹H and ¹³C NMR spectra were recorded in DMSO-*d*₆, CDCl₃ deuterated solvent on a Bruker Avance-III 400 MHz NMR spectrometer with operational frequencies 400 and 100 MHz, respectively. Chemical shift (δ) values are reported in parts per million (ppm), and coupling constants (*J*) are reported in Hz. The signal of residual solvents in DMSO-*d*₆ (2.50 ppm) and CDCl₃ (7.26 ppm) has been used for internal calibration in ¹H NMR, whereas in ¹³C NMR signal of DMSO-*d*₆ (39.52 ppm) CDCl₃ (77.16 ppm) and has been used for calibration. The signal multiplicities are abbreviated as singlet (s), doublet (d), triplet (t), doublet of doublets (dd), multiplet (m), overlapping (o) and broad (br).

HRMS: High-resolution mass spectra (HRMS) have been recorded using Waters Synapt G2- Si Q-TOF mass spectrometer. The ionization for those samples has been done using the electrospray ionization (ESI) method, and the detections were done in both positive and negative modes.

Melting points (MPs): Melting points were recorded on the SMP20 melting point apparatus and are uncorrected.

FT-IR studies: FT-IR spectra were recorded as a neat solid on a Bruker Alpha ZnSe ATR spectrometer in a transmittance mode.

UV-Vis spectroscopy: All the spectroscopic and sensing studies have been carried out by using Cary 60 and Cary 3500 UV-Vis spectrophotometers from Agilent technology. All studies were done in the solution phase in UV grade DMSO and Mili-Q water. Kinetics studies for urease activity was done in a scanning kinetics mode using multicell holder assembly.

Fluorescence spectroscopy: Fluorescence measurements were carried out on a Cary Eclipse fluorescence spectrophotometer. All studies were done in the solution phase in UV grade DMSO and Mili-Q water.

Strip Test

Whatman filter paper strips of 5 cm height and 1.5 cm width were made. These paper strips were dipped in 500 μ M solution of **P1** in THF and left for air-drying for 24 hours.

Agarose Gel

A 0.5 wt% agarose gel was made by mixing the probe **P1** molecule in a DMSO:H₂O (2:8 v/v) combination.

For amino acid detection: About 50 mg of agarose powder was added in 4 ml water, which was then heated to 100 °C until a uniform homogenous solution was formed. After allowing the agarose solution to cool, 1 ml of probe **P1** solution (40 μM in DMSO) was added. In order to achieve gelation, 500 μl volume of this mixture was placed in glass vials and kept standing at room temperature for 30 minutes.

For urea detection: About 15 mg of agarose powder was added in 2.4 ml water, then heated to 100 °C until a uniform homogenous solution was formed. After allowing the agarose solution to cool, 0.6 ml of probe **P1** solution (40 μM in DMSO) and urease (20 nM, 12 μl) were added. To achieve gelation, the mixture was poured into a Petri dish, and a capillary was placed at the center to create space for sampling purposes. After allowing it to stand at room temperature for 30 minutes, the capillary was removed, and the cavity was used to place urea and urine samples.

Image analysis

Pictures were clicked at different time interval during experiments and analysed with ImageJ software. A line was drawn from centre of cavity to end of the dish and plot profile was generated after scaling. Then 0.2 mm distance was subtracted from all images to exclude the radius of cavity and distances reported here are average of distance measured in various directions.

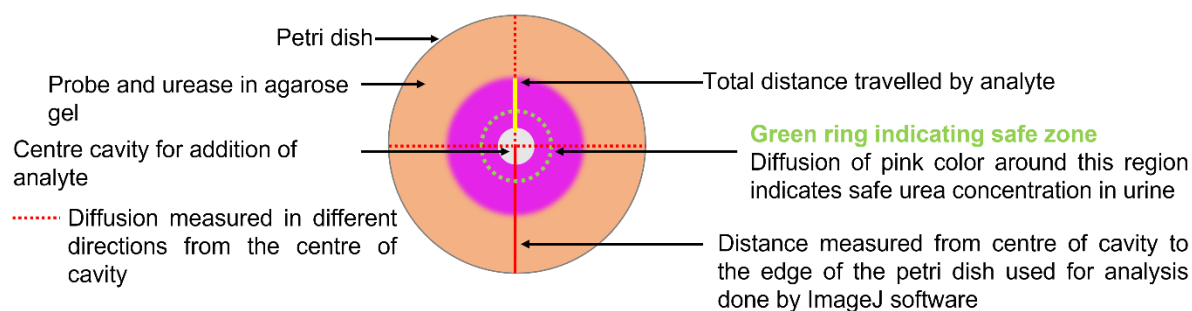


Figure S1.1. Schematic representation of the image analysis and estimation of urea based on the color diffusion.

S2. Spectroscopic studies

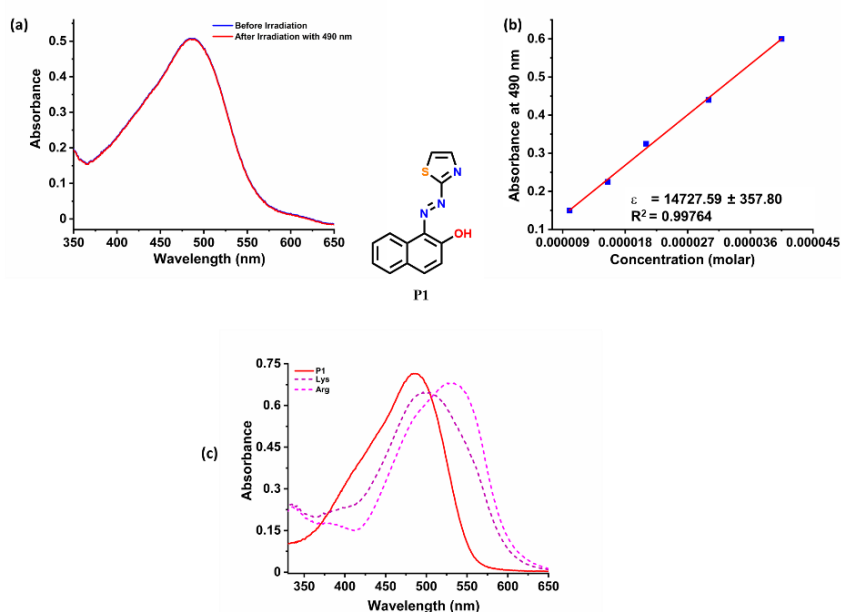


Fig S2.1. UV-Vis spectroscopic data of **P1**: (a) Photoswitching behaviour of **P1** before and after irradiation with 490 nm (no photoisomerization was observed); (b) Estimation of the molar absorption coefficient for π - π^* absorption maxima; (c) Absorption spectral changes of **P1** (40 μ M) upon addition of 10 eq. arginine and lysine.

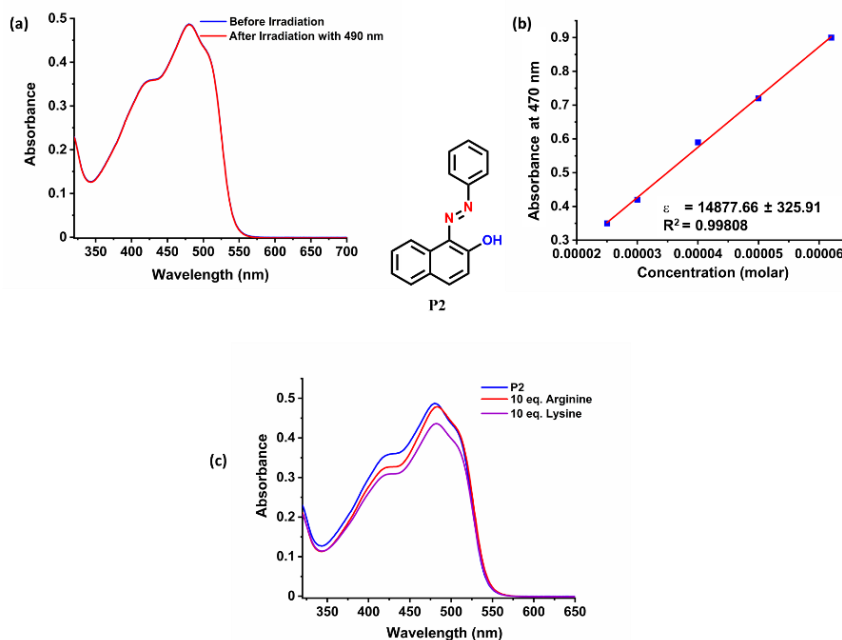


Fig S2.2. UV-Vis spectroscopic data of **P2**: (a) Photoswitching behaviour of **P2** before and after irradiation with 470 nm (no photoisomerization was observed); (b) Estimation of the molar absorption coefficient for π - π^* absorption maxima; (c) Absorption spectral changes of probe **P2** (30 μ M) upon adding 10 eq. arginine and lysine.

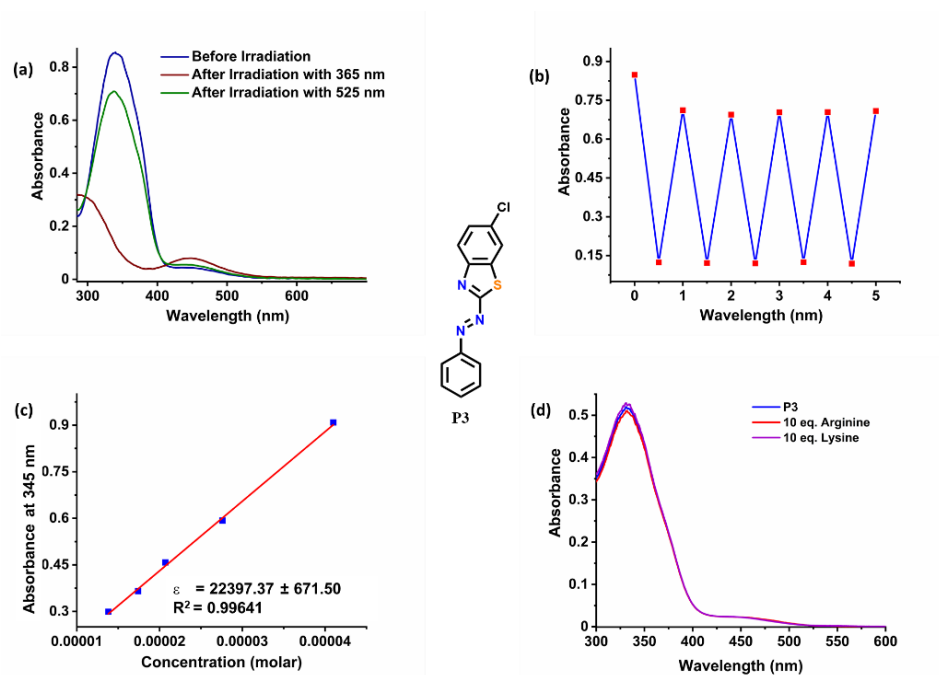


Fig S2.3. UV-Vis spectroscopic data of **P3**: (a) Photoisomerization of probe **P3** in DMSO; (b) Forward and reverse photoisomerization of **P3** upto five cycles; (c) Estimation of the molar absorption coefficient for π - π^* absorption maxima; (d) Absorption spectral changes of probe **P3** (28 μ M) upon adding 10 eq. arginine and lysine.

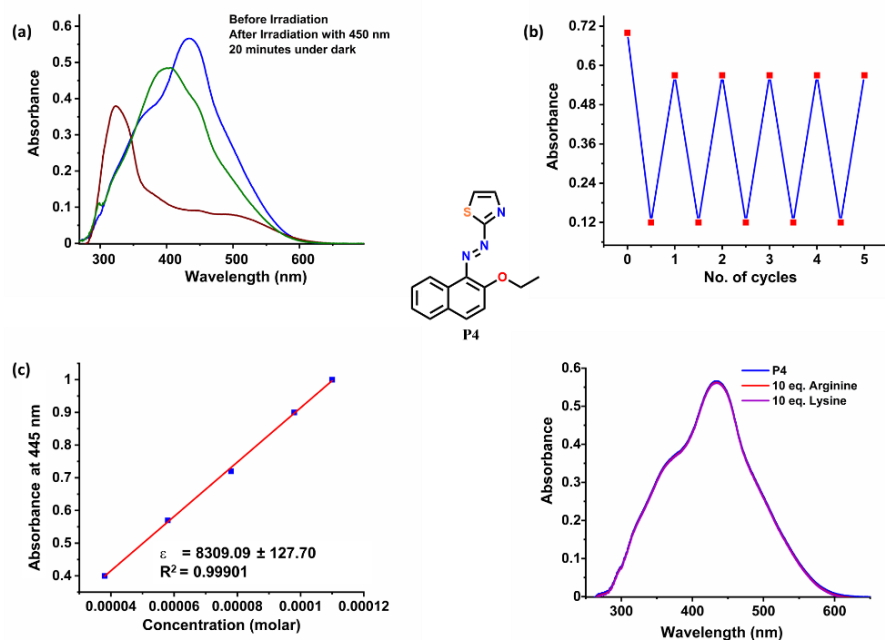


Fig S2.4. UV-Vis spectroscopic data of **P4**: (a) Photoisomerization of probe **P4** in DMSO; (b) Forward and reverse photoisomerization of **P4** upto five cycles; (c) Estimation of the molar absorption coefficient for π - π^* absorption maxima; (d) Absorption spectral changes of probe **P4** (60 μ M) upon adding 10 eq. arginine and lysine.

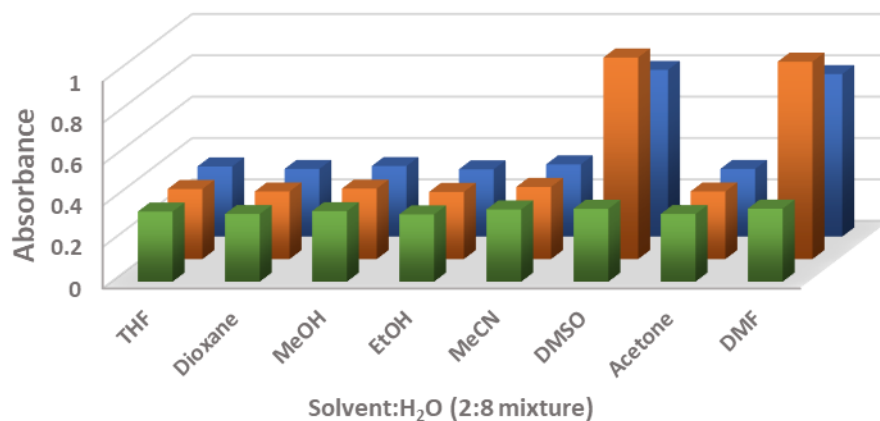


Fig S2.5. Effects of solvent in the detection of arginine (in blue) and lysine (in orange) (10 eq. of analytes were added).

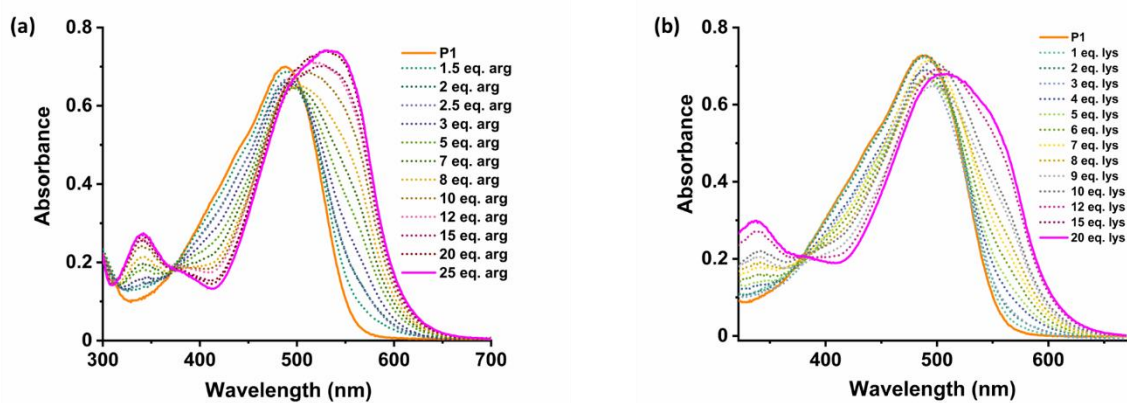


Fig S2.6. Absorption spectral changes of **P1** during titration with different equivalents of (a) arginine; (b) lysine.

S3. Quantitative analysis

A stock solution of probe **P1** (200 μM) in DMSO was prepared. The solution was used for all spectroscopic studies by appropriate dilution. For titration experiments, aqueous solutions of amino acids (500 μM each) and urea (20 mM) were prepared. All the UV-vis experiments were carried out in DMSO:H₂O (2:8 v/v, with phosphate buffer at a pH = 7.2) solution. Changes in the UV-vis spectra of the synthesized compounds were recorded on addition of analytes (arginine, lysine and urea) while keeping the probe concentration constant (40 μM) in all experiments. All the fluorescence spectroscopic experiments were carried out in DMSO/H₂O (2:8 v/v, with phosphate buffer at a pH = 7.2) solution. The fluorescence spectral measurements, all the samples were excited at 490 nm. Limit of detection (LOD) and binding constants K_a were calculated from the slope of the linear calibration plot.^{1,2} The stoichiometric ratio was calculated by Job's plot using the continuous variation method.¹ For Job's plot identical concentration solutions of probe **P1** and analytes (arginine and lysine) were prepared. Various solutions were prepared by changing the mole fractions of **P1** and arginine and lysine (separately) by keeping the total molar concentration constant. Absorbance changes were plotted against the mole fraction change to obtain the binding ratio.

Limit of detection (LOD) was calculated by using the formula:

$$\text{LOD} = 3.3 \times \sigma/m,$$

where σ = standard deviation, and m = slope.

The association constant or binding constant, K_a was calculated using the equation:

$$\frac{1}{A-A_0} = \frac{1}{\{K_a(A_{max}-A_0)[C]\}} + \frac{1}{(A_{max}-A_0)}$$

where A_0 and A are the absorbance of the probe in the absence and the presence of the analyte; A_{max} is absorbance in the presence of $[C]_{max}$, $[C]$ is concentration of the analyte, K_a is association constant (M^{-1}). By plotting $1/[C]$ against $1/(A-A_0)$, K_a could be determined from the slope of the resulting linear plot.

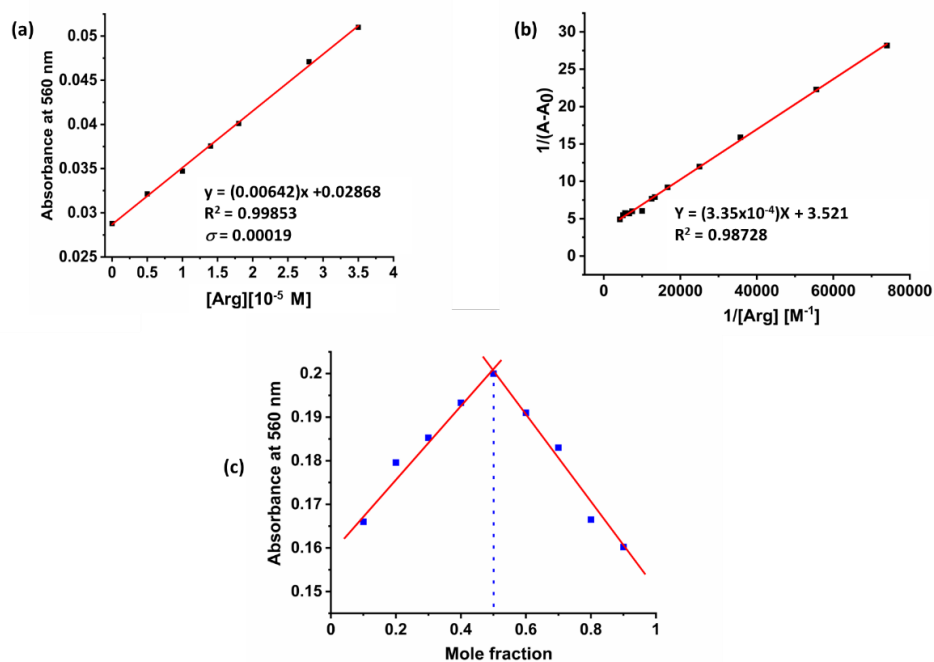


Figure S3.1. (a) Linear calibration plot of absorbance vs concentration of arginine for the determination of LOD; (b) Benesi-Hildebrand lot of absorbance of **P1** at 560 nm against increasing concentrations of arginine; (c) Job's plot of **P1** for arginine.

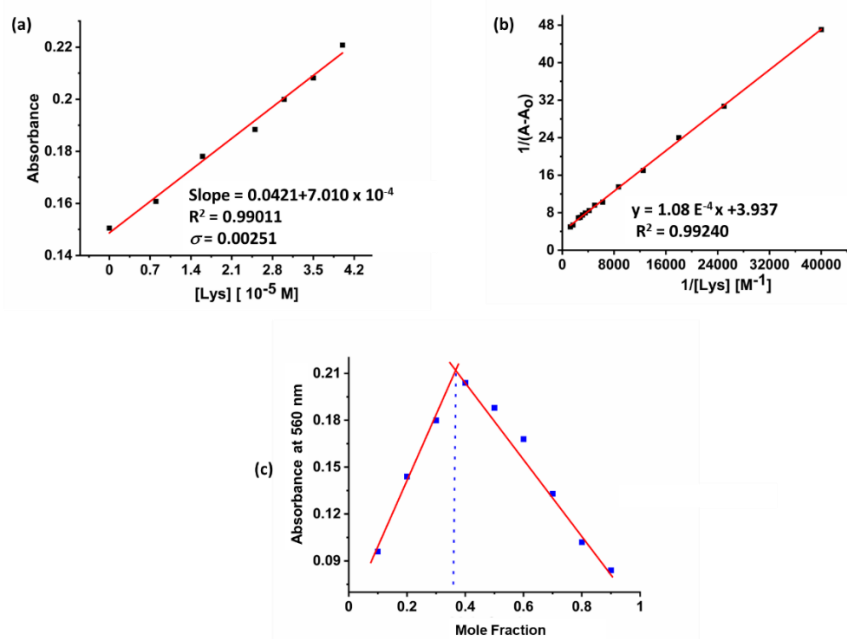


Figure S3.2. (a) Linear calibration plot of absorbance vs concentration of lysine for the determination of LOD; (b) Benesi-Hildebrand Plot of absorbance of **P1** at 560 nm against increasing concentration of lysine; (c) Job's plot of **P1** for lysine.

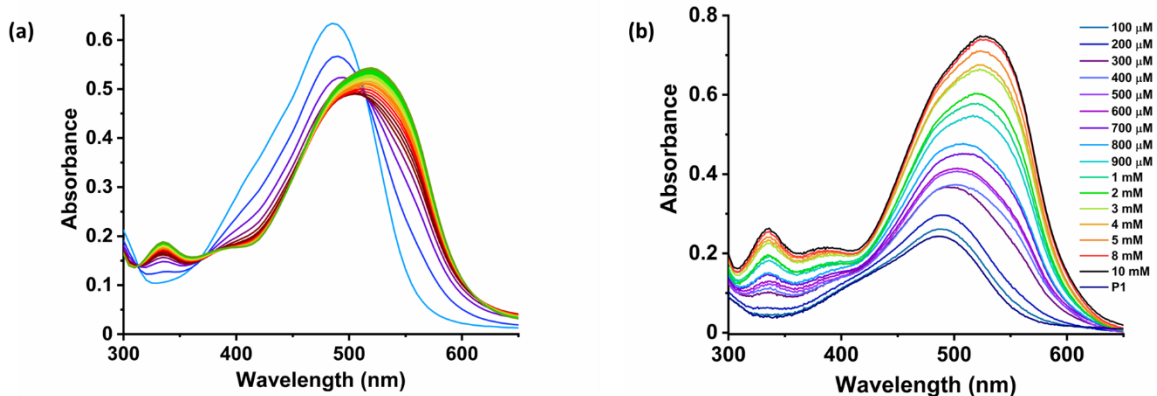


Figure S3.3. (a) Scanning kinetics to follow urea hydrolysis by probe **P1** in the presence of 20 nM urease for 30 minutes (urea 500 μ M, 40 μ M **P1**); (b) Titration between the probe **P1** and urea in the presence of urease (20 nM urease, 40 μ M **P1**).

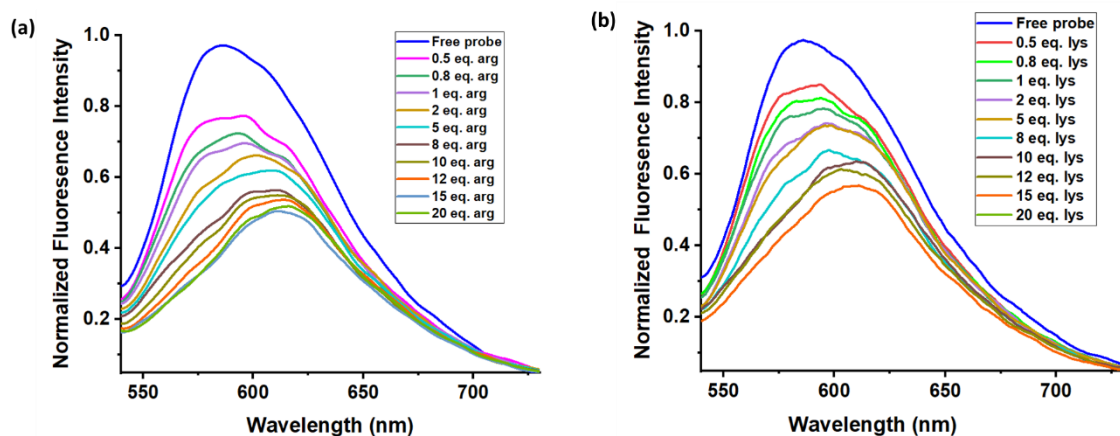


Figure S3.4. Fluorescence emission in probe **P1** (40 μ M) without and with the increasing concentrations of (a) Arginine; (b) Lysine.

S4. Mechanism of sensing

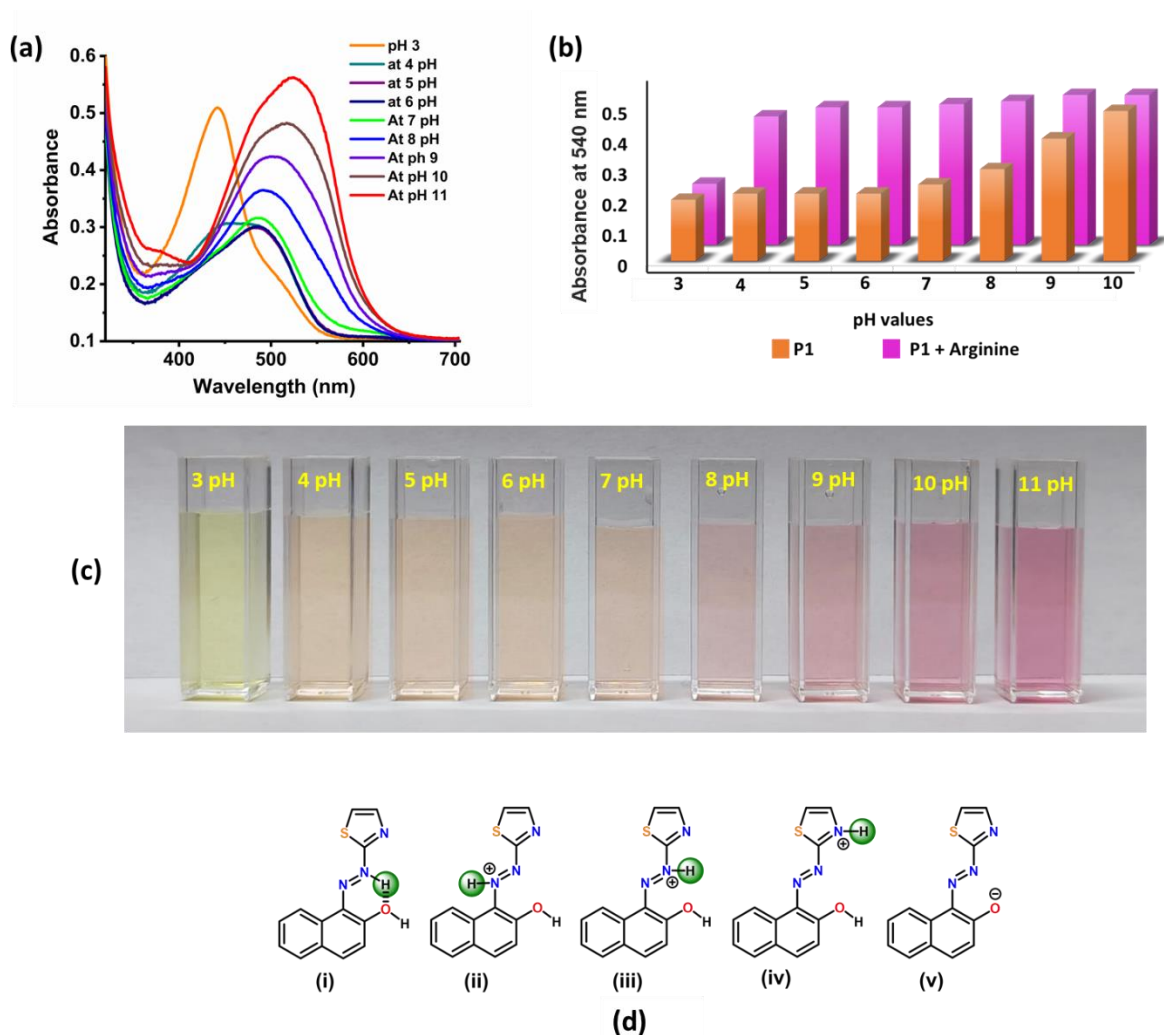


Figure S4.1. Effect of pH in sensing: (a) Spectral changes of probe **P1** at different pH; (pH adjustment in the **P1** in DMSO-water (2:8) mixture in phosphate buffer was made using 1M each NaOH and HCl solutions); (b) Histograms depicting the effect of pH in the absorption at 540 nm in the absence and the presence of 10 eq. arginine; (c) Photographs depicting color changes in the probe **P1** upon changing the pH in the range 3-11 (all the experiments were performed using 10 mM phosphate buffer and 40 μ M solution of **P1**); (d) Possible protonated and deprotonated species.

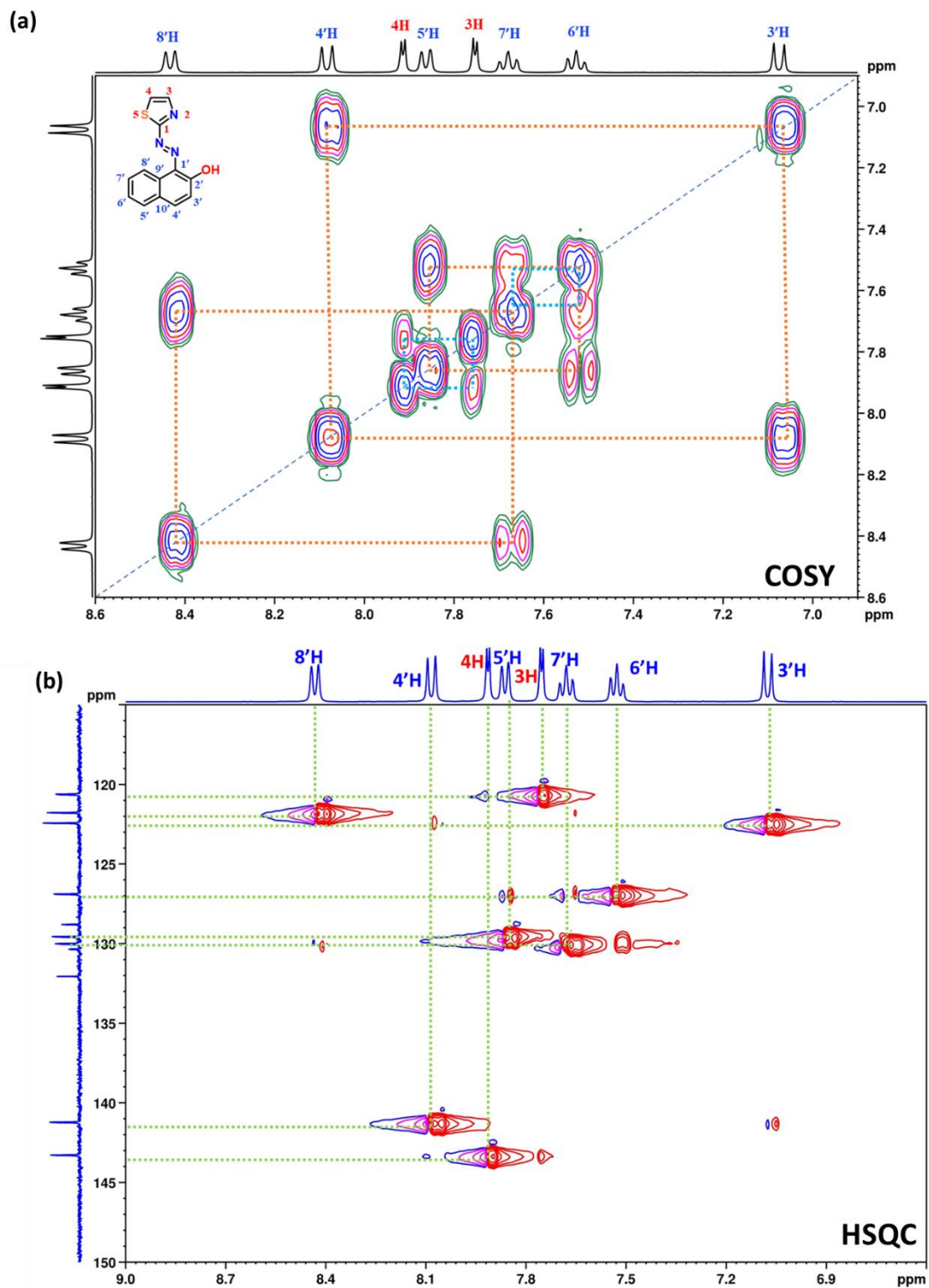


Figure S4.2. 2D NMR spectra of free probe **P1** in DMSO- d_6 (a) ^1H - ^1H COSY, and (b) HSQC.

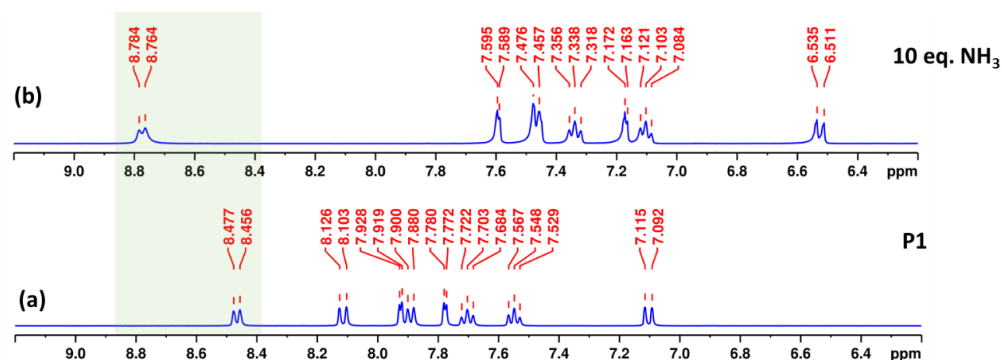


Figure S4.3. Analysis of binding between the probe **P1** (5 mM) and ammonia using $^1\text{H-NMR}$ spectroscopy (in $\text{DMSO-}d_6$): (a) **P1**, and (b) **P1** in the presence of 10 eq. of ammonia (as aqueous solution).

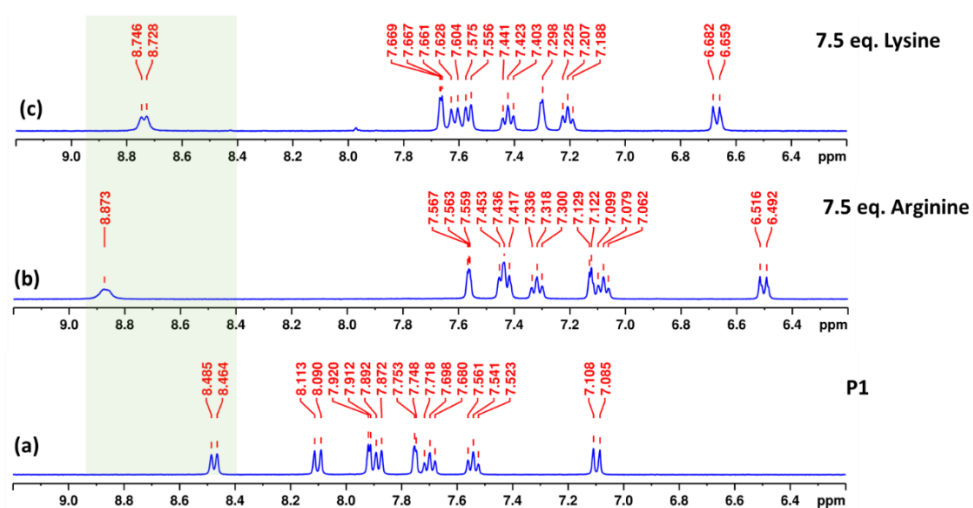


Figure S4.4. Analysis of binding between the probe **P1** (5 mM) and ammonia using $^1\text{H-NMR}$ spectroscopy (in $\text{DMSO-}d_6:\text{D}_2\text{O}$, 9.5:0.5): (a) **P1**; (b) **P1** in the presence of 7.5 eq. arginine, and (c) **P1** in the presence of 7.5 eq. lysine.

S5. Scope of detection and studies in gel

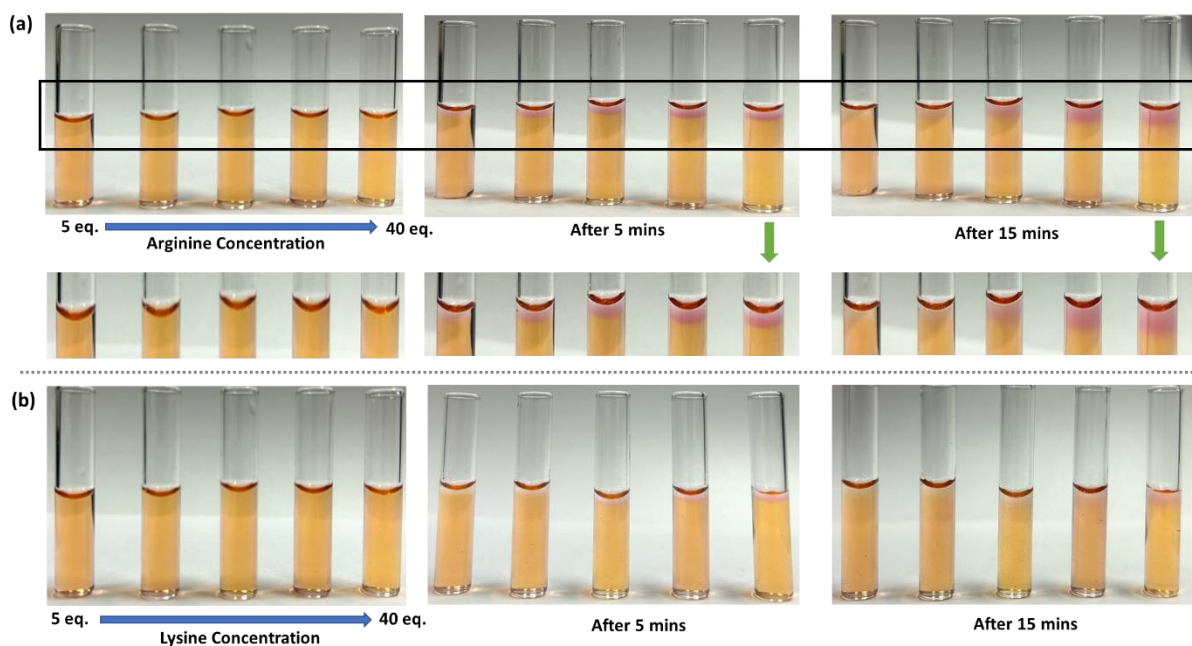


Figure S5.1. Detection of arginine and lysine in agarose gel medium (probe **P1** concentration 40 μM): Images indicating prominent color change and diffusion in the presence of varying concentrations of (a) arginine solution in the gel over time (the zoomed portion is also depicted for clarity); (b) lysine solution in gel over time; (concentration of arginine and lysine from left to right 5 (200 μM), 10 (400 μM), 20 (800 μM), 30 (1200 μM), 40 (1600 μM) eq.).

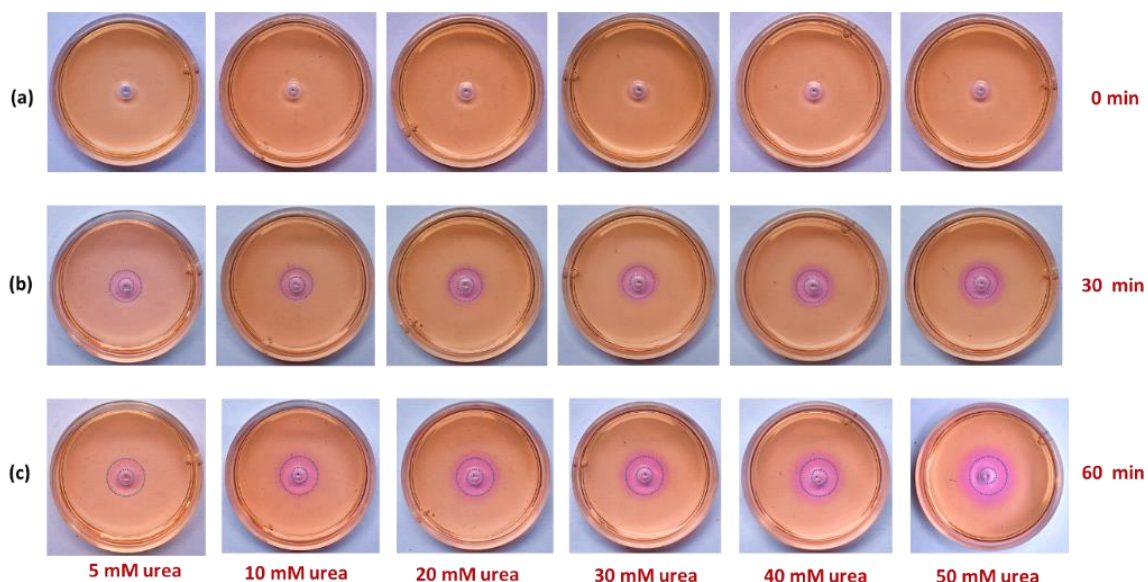


Figure S5.2. Images depicting the visual detection of urea through color diffusion at different concentrations of urea (in the range 5 to 50 mM): The diffusion of pink band in the gel at (a) 0, (b) 30, and (c) 60, min.

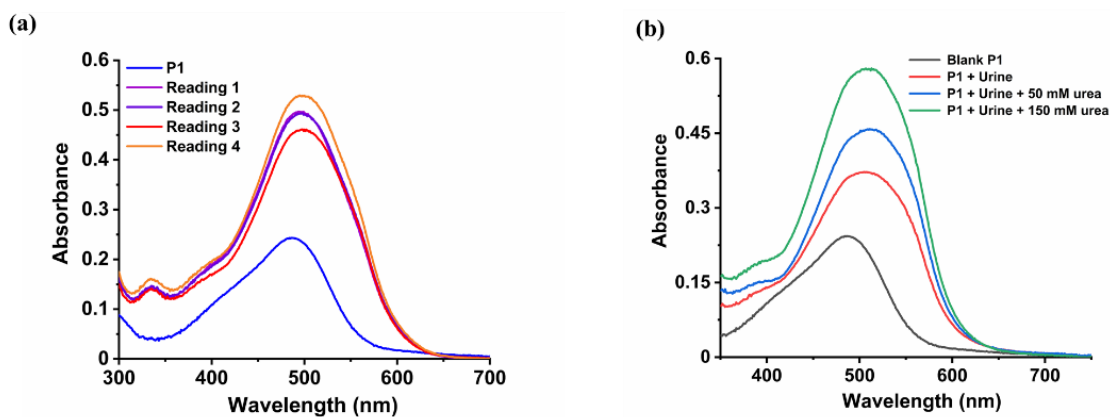


Figure S5.3. (a) Changes in absorption spectra of **P1** in the presence of urine only (average of 4 readings is used for estimation of urea, under enzymatic condition); (b) Changes in absorption spectra of **P1** in the presence of different urea concentration containing urine samples.

Table S5.1. Summary table of recovery of urea spiked in urine sample.

| Sample No. | Spiked urea concentration (mM) | Total urea concentration (mM) | Urea concentration found (mM) | Recovery % ^a |
|------------|--------------------------------|-------------------------------|-------------------------------|-------------------------|
| i | 0 | 177.3 | 177.3 ± 2.30 | 0 |
| ii | 50 | 227.3 | 227.5 ± 6.14 | 100.4 |
| iii | 150 | 327.3 | 325.9 ± 5.21 | 98.9 |

^aUrea concentration recovered in percentage after spiking.

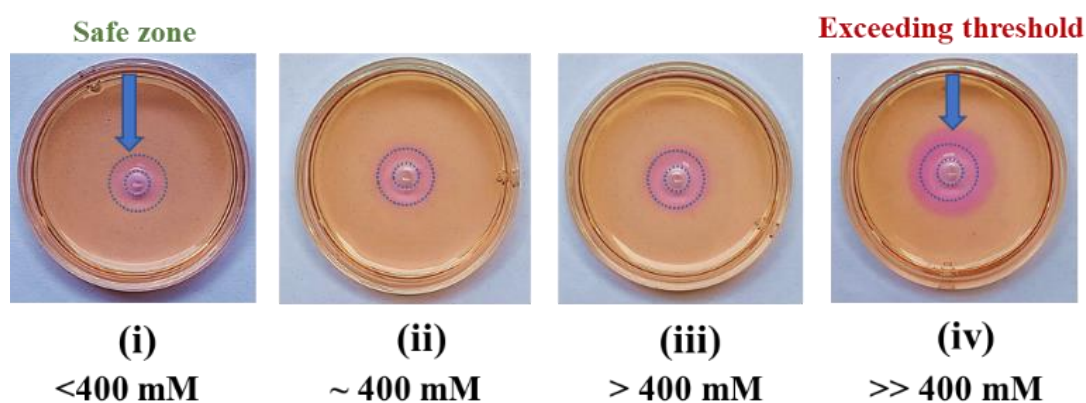


Figure S5.4. Images depicting the visual detection of spiked urea in urine through color diffusion in the gel after 60 minutes.

Table S5.2. Summary table of diffusion distance and recovered concentration for urea spiked in urine sample.

| Sample No. | Spiked urea concentration (mM) | Total urea concentration (mM) | Diffusion length (mm) | Estimated urea concentration (mM) |
|-------------------|---------------------------------------|--------------------------------------|------------------------------|--|
| i | 0 | 177.3 | 1.58 | (160-200) |
| ii | 200 | 377.3 | 2.75 | (360-400) |
| iii | 500 | 677.3 | 3.49 | (650-700) |
| iv | 1500 | 1677.3 | 4.49 | (1640-1700) |

S6. Long-term stability, reusability and pH stability of probe

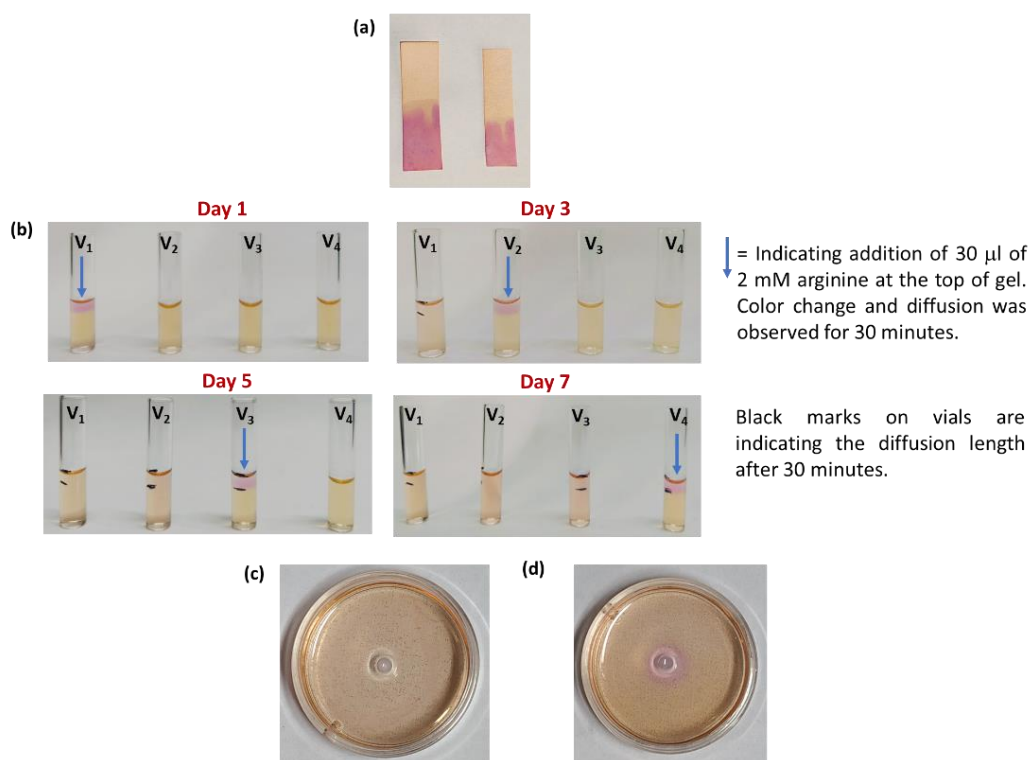


Figure S6.1. Test for long-term stability of the probe. Images taken after (a) Fresh and a month-old strip dipped in arginine solution (5 mM) exhibiting similar color change; (b) Detection of arginine for 7 days in gel medium (40 μM probe in agarose gel; concentration of arginine used are specified at the top); Images of the Petri dish having probe in agarose gel after 24 hours: (c) Blank sample without urea, and (d) After addition of urea 20 mM urea with 20 nM urease.

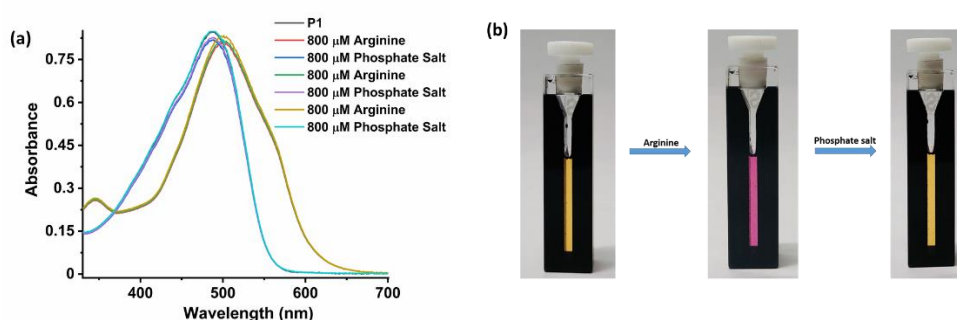


Figure S6.2. Test for reusability of the probe. (a) UV-Vis spectral data demonstrating three cycles of alternative addition of arginine (800 mM in water) and H_2PO_4^- (800 mM in water) to the probe in DMSO- H_2O (2:8; 60 mM). (b) Images depicting the probe solution (orange), after addition of arginine (pink) and after the addition of H_2PO_4^- (regeneration of orange).

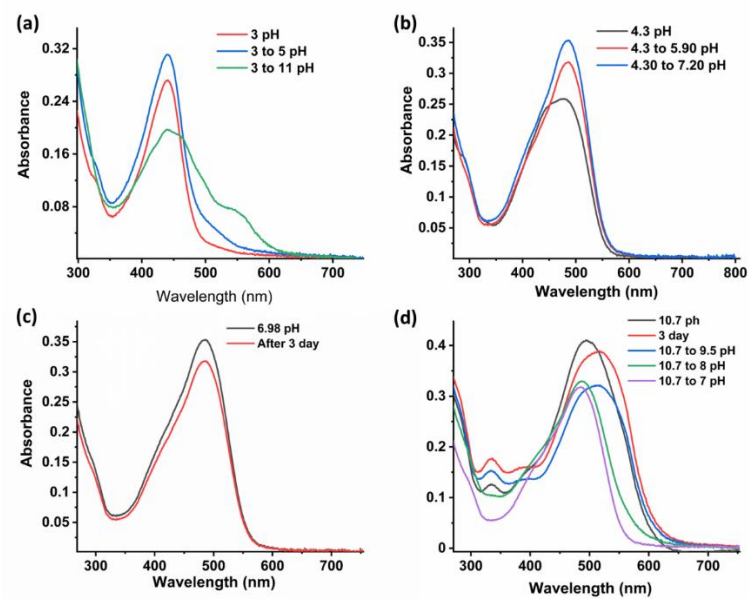


Figure S6.3. Changes in absorption spectrum at different pH and reversibility of absorption changes by pH variation.

S7. Computational details

All density functional theory (DFT) was performed using the Gaussian16 (Revision C.01) suite of quantum chemical programs.³ The geometry optimizations of the probe and its interaction with the ammonia, and amino acids (arginine, lysine) were carried out using hybrid generalized gradient approximation, B3LYP functional^{4,5} including Grimme's Beck–Johnson damping dispersion correction⁶ D3 (BJ) with and 6-311G(d,p) basis set⁷ for all the other atoms. Time-dependent DFT calculations were performed using the Polarizable Continuum Model (PCM)⁷ using the integral equation formalism (IEFPCM).⁸ The quantum theory of atoms in molecules (QTAIM)⁹ and non-covalent interaction analysis¹⁰ were performed using the Multiwfn program.¹¹ To acquire the isosurfaces for the non-covalent interaction (NCI) VMD software¹² was used and reduced density gradient (RDG) plots were obtained from the Multiwfn outputs.

To gain insights into the origin of the shifts and color changes, density functional theory (DFT at B3LYP-D3/6-311G(d,p) level of theory) electronic structure calculations were performed by optimizing the probe **P1** capable of exhibiting tautomerism and different conformations (**Figure S7.1**) Afterwards, the complexes of **P1** with ammonia and amino acids (arginine and lysine) were analyzed. In this regard, various modes of complexation between them were considered, and the corresponding geometries were fully optimized to minima and the non-covalent interactions stabilizing them were identified (**Figures S7.1-S7.5**). The non-covalent interaction (NCI) analysis predicted hydrogen bonding interactions involving the azo group of the probe **P1** with ammonia and arginine. However, in lysine, the interactions are dominated by weak van der Waal's interaction and secondary hydrogen bonding interaction. Furthermore, different stoichiometric ratios (1:1 and 1:2) for complexation between them were also attempted. The binding energies of the complexes of **P1** are estimated with NH₃, Arg, and Lys to be -9.4, -27.6 and -32.5 kcal/mol, respectively.

Also, the minimum energy complexes were subjected to TD-DFT calculations to understand the electronic transitions associated with them. The **P1** exhibited an absorption maximum at 477 nm, which agrees with the experimental absorption maxima of 490 nm, and this peak is attributed to the transitions from the highest occupied molecular orbital (HOMO) to the lowest unoccupied molecular orbital (LUMO) corresponding to $\pi \rightarrow \pi^*$ transition. When complexed with arginine, a peak appears at 525 nm, supports the experimental absorption feature at 545 nm, and is assigned to HOMO-1 to LUMO ($n \rightarrow \pi^*$) (76%) transition and HOMO to LUMO $\pi \rightarrow \pi^*$ (21%) transition. A decreased HOMO-LUMO gap for the **P1**-Arg complex resulted in a redshift mainly arising from $n \rightarrow \pi^*$ and $\pi \rightarrow \pi^*$ transitions in the **P1**-Arg complex (**Figures S7.6 and S7.7**). These trends are reflected in the absorption spectral features and corroborate well with the experimental findings.

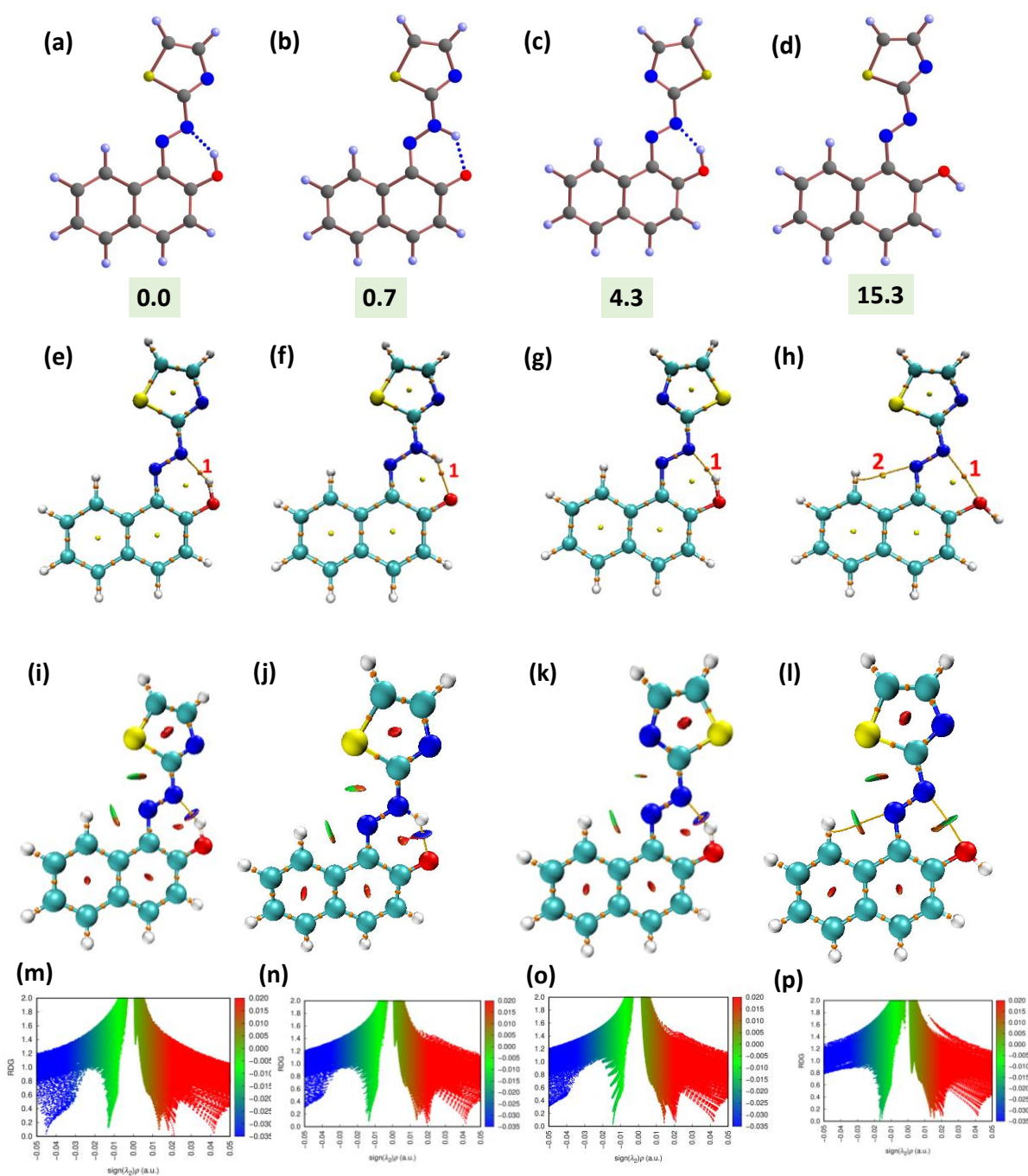


Figure S7.1. DFT-optimized conformers of **P1** (a) *E1-syn* (enol-form), (b) *E2-hydrazone* (keto-form), (c) *E3-syn* (enol-form), and (d) *E4-anti* (enol-form). Relative energy in kcal/mol is indicated below each conformer. (e-h) AIM computed topological diagrams for *E1-E4* (Color code:- gold: bond critical point; yellow: ring critical point, and green: cage critical point). (i-l) non-covalent interaction (NCI) plots for *E1-E4*; (m-p) reduced density gradient (RDG) scatter plots (The blue-colored spikes in the negative region of the scatter plot correspond to the hydrogen bonds, the red-colored spikes represent the strong repulsive interactions, and the green region indicates the van der Waals interaction).

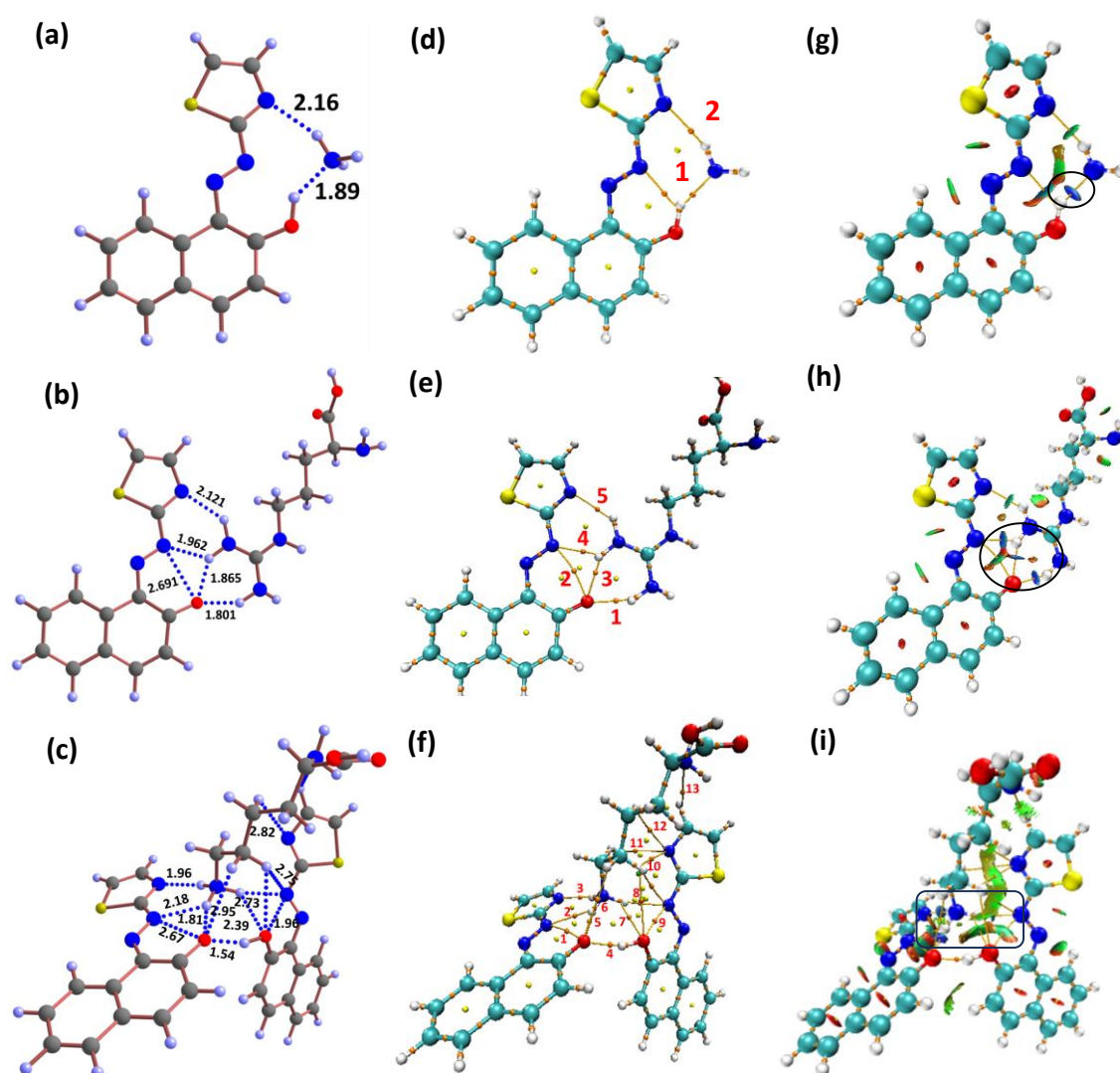


Figure S7.2. The optimized geometries of the most stable complex by the interaction between: (a) **P1** and ammonia; (b) **P1** and arginine (c) **P1** and lysine. The atomic contacts (blue color) represent various non-covalent interactions in Å; (d-f) Atoms in molecule (AIM) computed topological diagrams: (d) **P1** and ammonia; (e) **P1** and arginine and (f) **P1** and lysine; (g-i) Non-covalent interaction plot for: (g) **P1** and ammonia; (h) **P1** and arginine and (i) **P1** and lysine {color code for atoms: grey: carbon; blue: nitrogen; red: oxygen; yellow: sulphur: yellow (Color code for critical points:- gold: bond critical point; yellow: ring critical point, and green: cage critical point).

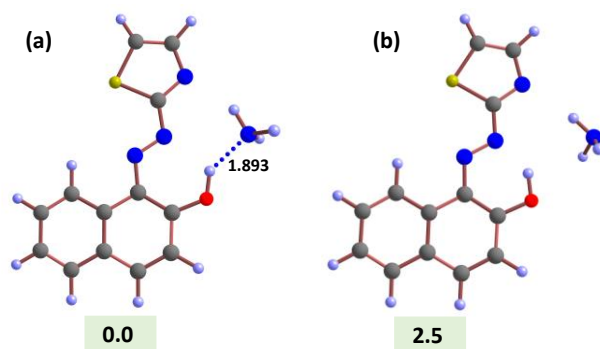


Figure S7.3. Various possible modes of interactions between **P1** and ammonia. Relative energy in kcal/mol is indicated below each conformer.

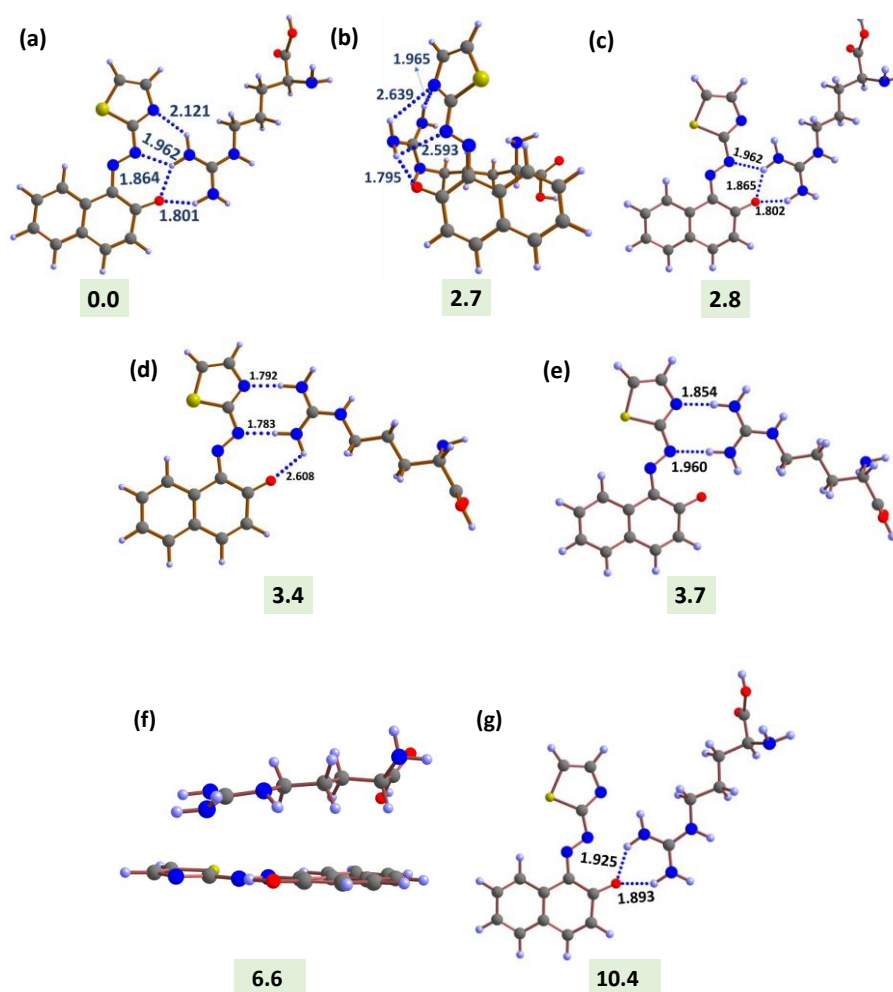


Figure S7.4. Various possible modes of interaction between **P1** and arginine. Relative energy in kcal/mol is indicated below each conformer.

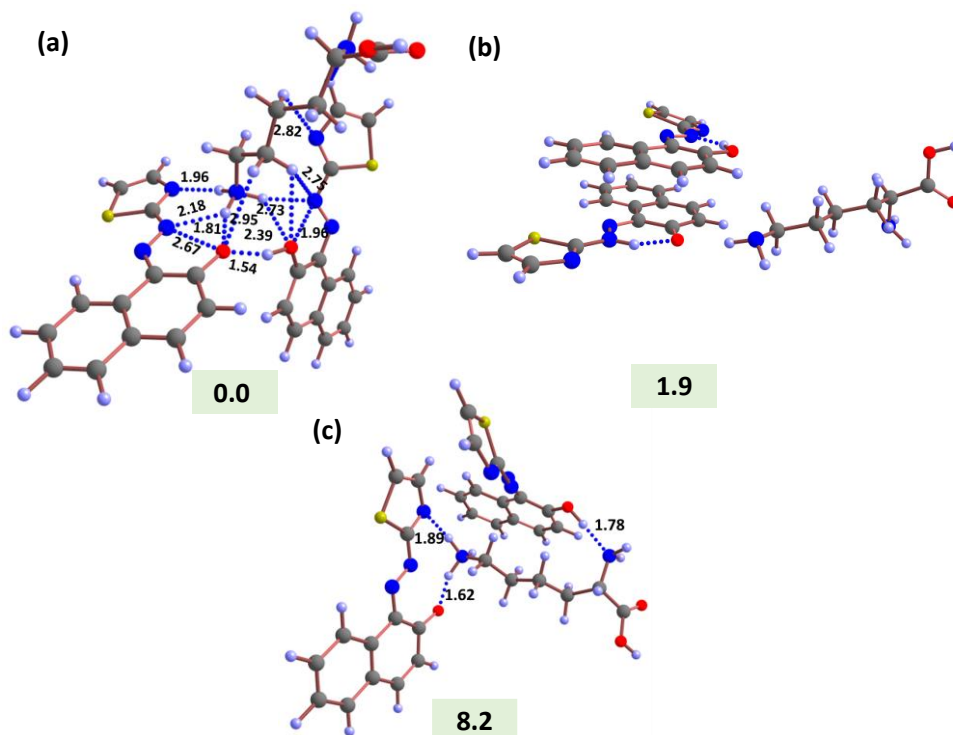


Figure S7.5. Various possible modes of interaction between P1 and lysine. Relative energy in kcal/mol is indicated below each complex.

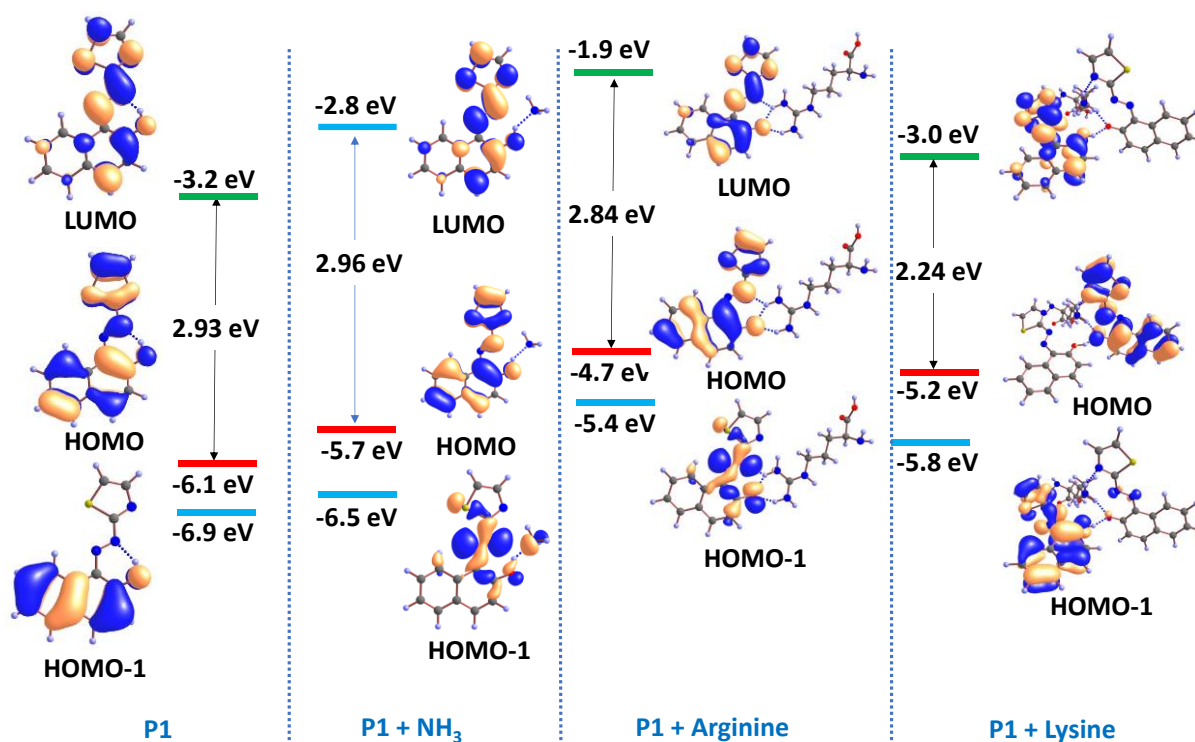


Figure S7.6. Frontier molecular orbitals of P1, P1+NH₃, P1+ Arginine, P1+Lysine

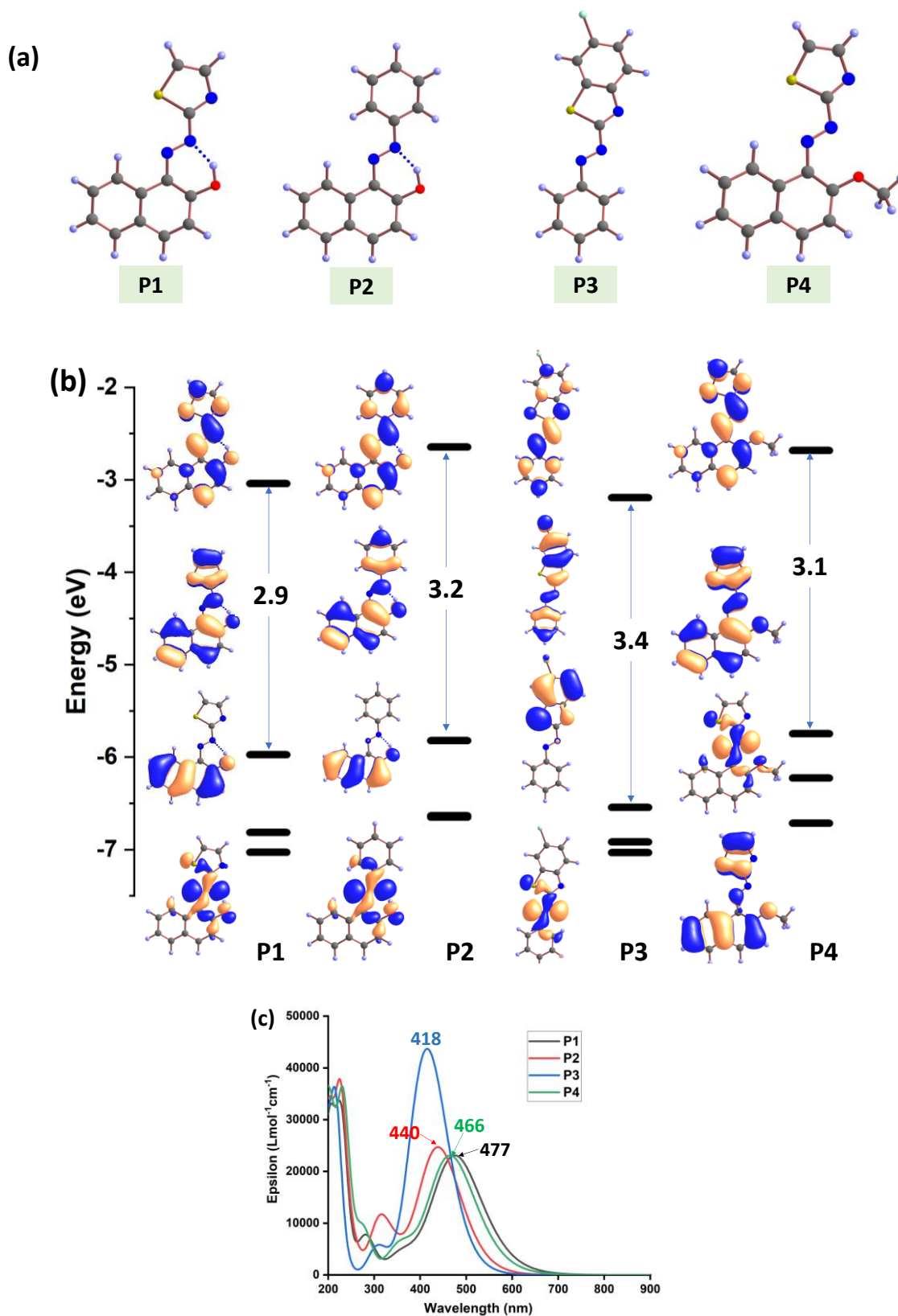


Figure S7.7. (a) DFT optimized geometries of probe **P1-P4**; (b) Frontier molecular orbitals of probes **P1-P4**. All orbital energies are in eV; (c) TD-DFT computed UV-Vis spectra for **P1-P4**.

Table S7.1. Topological parameters of different conformers at the bond critical point of *E1-E4*. The electron density [$\rho(r)$], Laplacian of electron density [$\nabla^2\rho(r)$], local electronic kinetic energy density [$G(r)$], local electronic potential energy density [$V(r)$], and interaction energy (E) values are indicated. The values for $\rho(r)$, $\nabla^2\rho(r)$, $G(r)$, and $V(r)$ are given in atomic units and for E , in kcal/mol.

| S. No. | BCP and type of interaction | Contact distance Å | $\rho(r)$ (au) | $\nabla^2\rho(r)$ (au) | $G(r)$ (au) | $V(r)$ (au) | E (kcal/mol) |
|------------------|-----------------------------|--------------------|----------------|------------------------|-------------|-------------|----------------|
| <i>E1</i> | | | | | | | |
| 1 | N...H | 1.671 | 0.0584 | 0.1227 | 0.0457 | -0.0610 | -19.15 |
| <i>E2</i> | | | | | | | |
| 1 | H...O | 1.739 | 0.0453 | 0.1500 | 0.0416 | -0.0456 | -14.31 |
| <i>E3</i> | | | | | | | |
| 1 | N...H | 1.671 | 0.0586 | 0.1224 | 0.0458 | -0.0610 | -19.06 |
| <i>E4</i> | | | | | | | |
| 1 | N...H | 2.623 | 0.0168 | 0.0742 | 0.0155 | -0.0126 | -3.94 |
| 2 | H...N | 2.405 | 0.0156 | 0.0686 | 0.0142 | -0.0113 | -3.55 |

Table S7.2. Topological parameters of different conformers at the bond critical point of **P1+NH₃**, **P1+Arginine**, and **P1+Lysine**. The electron density [$\rho(r)$], Laplacian of electron density [$\nabla^2\rho(r)$], local electronic kinetic energy density [$G(r)$], local electronic potential energy density [$V(r)$], and interaction energy (E) values are indicated. The values for $\rho(r)$, $\nabla^2\rho(r)$, $G(r)$, and $V(r)$ are given in atomic units and for E , in kcal/mol.

| S. No. | BCP and type of interaction | Contact distance Å | $\rho(r)$ (au) | $\nabla^2\rho(r)$ (au) | $G(r)$ (au) | $V(r)$ (au) | E (kcal/mol) |
|--------------------------|-----------------------------|--------------------|----------------|------------------------|-------------|-------------|----------------|
| P1+NH₃ | | | | | | | |
| 1 | N...H | 1.893 | 0.025 | 0.086 | 0.020 | -0.019 | -6.100 |
| 2 | H...N | 2.158 | 0.035 | 0.093 | 0.026 | -0.029 | -9.131 |
| P1+Arginine | | | | | | | |
| 1 | H...O | 1.801 | 0.033 | 0.129 | 0.031 | -0.030 | -9.482 |

| | | | | | | | |
|------------------|-------|-------|-------|-------|-------|--------|---------|
| 2 | O...N | 2.691 | 0.018 | 0.067 | 0.015 | -0.013 | -4.058 |
| 3 | O...H | 1.865 | 0.031 | 0.115 | 0.028 | -0.027 | -8.453 |
| 4 | H...N | 1.962 | 0.030 | 0.102 | 0.025 | -0.025 | -7.755 |
| 5 | H...N | 2.121 | 0.021 | 0.069 | 0.016 | -0.015 | -4.676 |
| P1+Lysine | | | | | | | |
| 1 | N...O | 2.669 | 0.019 | 0.071 | 0.016 | -0.014 | -4.242 |
| 2 | N...H | 2.178 | 0.020 | 0.075 | 0.017 | -0.015 | -4.714 |
| 3 | N...H | 1.963 | 0.030 | 0.087 | 0.023 | -0.024 | -7.384 |
| 4 | O...H | 1.540 | 0.066 | 0.171 | 0.060 | -0.076 | -23.995 |
| 5 | H...O | 1.813 | 0.034 | 0.120 | 0.030 | -0.031 | -9.584 |
| 6 | H...O | 2.946 | 0.004 | 0.016 | 0.003 | -0.002 | -0.608 |
| 7 | H...O | 2.385 | 0.012 | 0.046 | 0.010 | -0.008 | -2.375 |
| 8 | H...O | 2.735 | 0.006 | 0.021 | 0.004 | -0.003 | -0.921 |
| 9 | O...N | 2.651 | 0.017 | 0.072 | 0.015 | -0.013 | -3.965 |
| 10 | H...N | 2.757 | 0.008 | 0.025 | 0.005 | -0.004 | -1.172 |
| 11 | H...N | 2.697 | 0.009 | 0.026 | 0.005 | -0.004 | -1.328 |
| 12 | H...N | 2.824 | 0.006 | 0.020 | 0.004 | -0.003 | -0.900 |
| 13 | N...H | 2.961 | 0.005 | 0.017 | 0.003 | -0.002 | -0.728 |

Table S7.3. Excited states of **P1** with oscillator strengths greater than 0.05 calculated by TD-DFT

| State number | λ (nm) | ΔE (eV) | f | Transition character |
|--------------|----------------|-----------------|-------|---------------------------------|
| 1 | 477 | 2.598 | 0.559 | HOMO \rightarrow LUMO (99%) |
| 3 | 393 | 3.149 | 0.065 | HOMO-1 \rightarrow LUMO (98%) |
| 4 | 353 | 3.503 | 0.084 | HOMO-3 \rightarrow LUMO (96%) |
| 7 | 282 | 4.385 | 0.171 | HOMO-4 \rightarrow LUMO (96%) |
| 13 | 229 | 5.401 | 0.416 | HOMO \rightarrow LUMO+3 (42%) |

Table S7.4. Excited states of **P1-Arginine** with oscillator strengths greater than 0.04 calculated by TD-DFT

| State number | λ (nm) | ΔE (eV) | f | Transition character |
|--------------|----------------|-----------------|--------|--|
| 1 | 540 | 2.293 | 0.5626 | HOMO-1 \rightarrow LUMO (77%) HOMO \rightarrow LUMO (10%) |
| 2 | 484 | 2.556 | 0.4425 | HOMO-1 \rightarrow LUMO (10%) HOMO \rightarrow LUMO (78%) |
| 3 | 382 | 3.243 | 0.0736 | HOMO-2 \rightarrow LUMO (96%) |
| 11 | 271 | 4.567 | 0.1045 | HOMO-5 \rightarrow LUMO+1 (72%) |

Table S7.5. Excited states of **P1**-Lysine with oscillator strengths greater than 0.04 calculated by TD-DFT

| State number | λ (nm) | ΔE (eV) | f | Transition character |
|--------------|----------------|-----------------|-------|-----------------------------------|
| 2 | 556 | 2.228 | 0.206 | HOMO-1 \rightarrow LUMO (79%) |
| 4 | 480 | 2.580 | 0.456 | HOMO \rightarrow LUMO+1 (92%) |
| 5 | 464 | 2.667 | 0.119 | HOMO-2 \rightarrow LUMO (88%) |
| 7 | 432 | 2.865 | 0.187 | HOMO-7 \rightarrow LUMO (30%) |
| 9 | 393 | 3.153 | 0.095 | HOMO-3 \rightarrow LUMO+1 (95%) |

S8. Spectral characterization (^1H , ^{13}C NMR data)

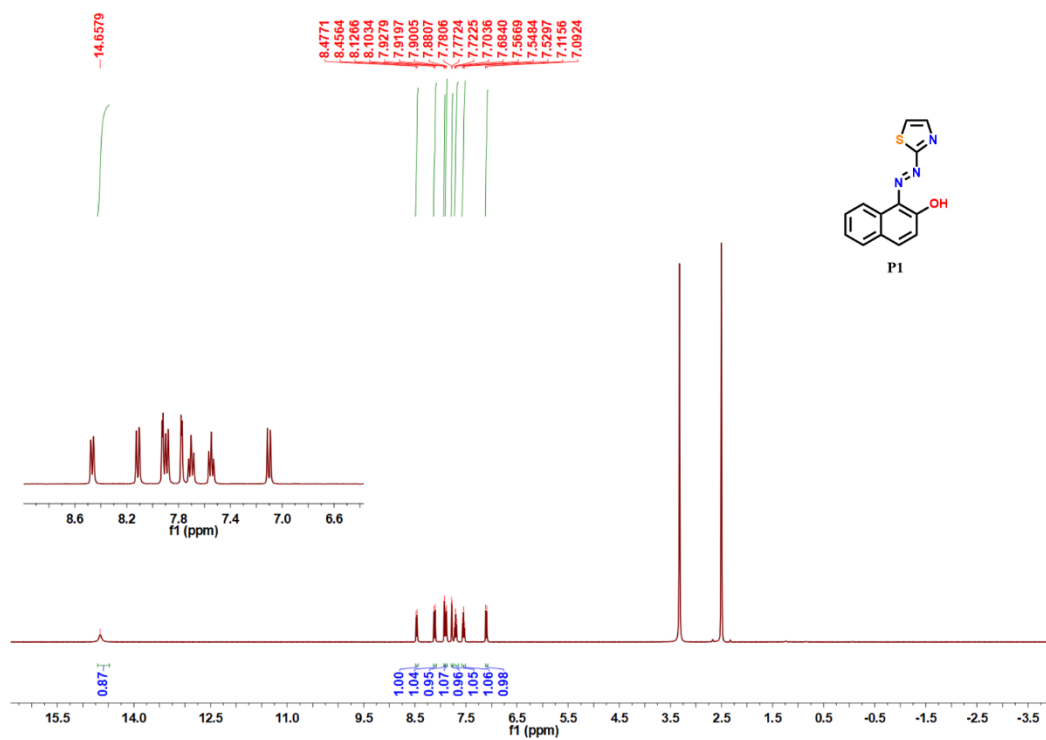


Figure S8.1. ^1H NMR (400 MHz) spectrum of P1 in $\text{DMSO-}d_6$.

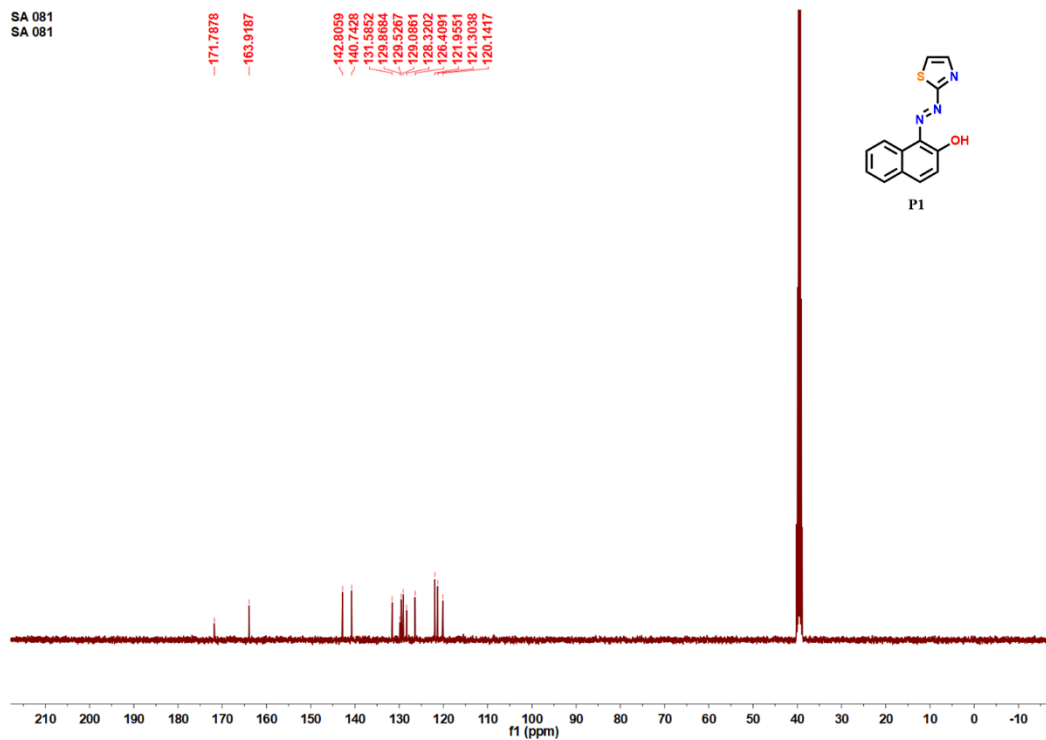


Figure S8.2. ^{13}C NMR (100 MHz) spectrum of P1 in $\text{DMSO-}d_6$.

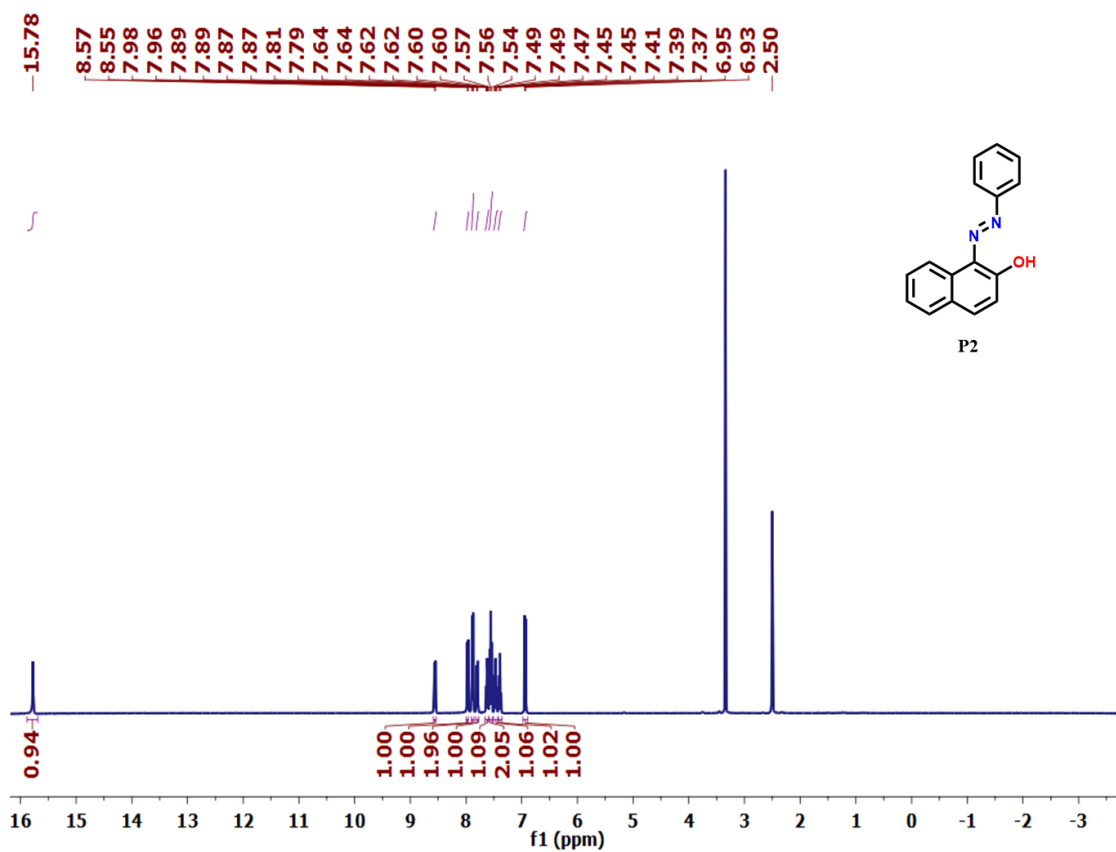


Figure S8.3. ^1H NMR (400 MHz) spectrum of **P2** in $\text{DMSO-}d_6$.

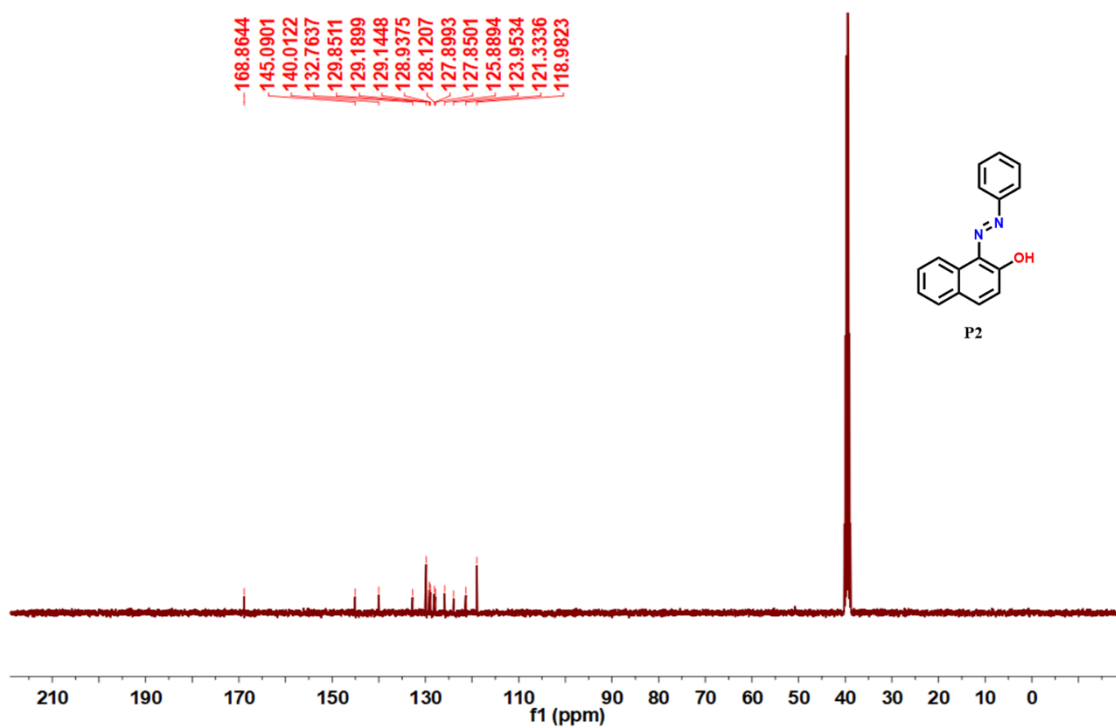


Figure S8.4. ^{13}C NMR (100 MHz) spectrum of **P2** in $\text{DMSO-}d_6$.

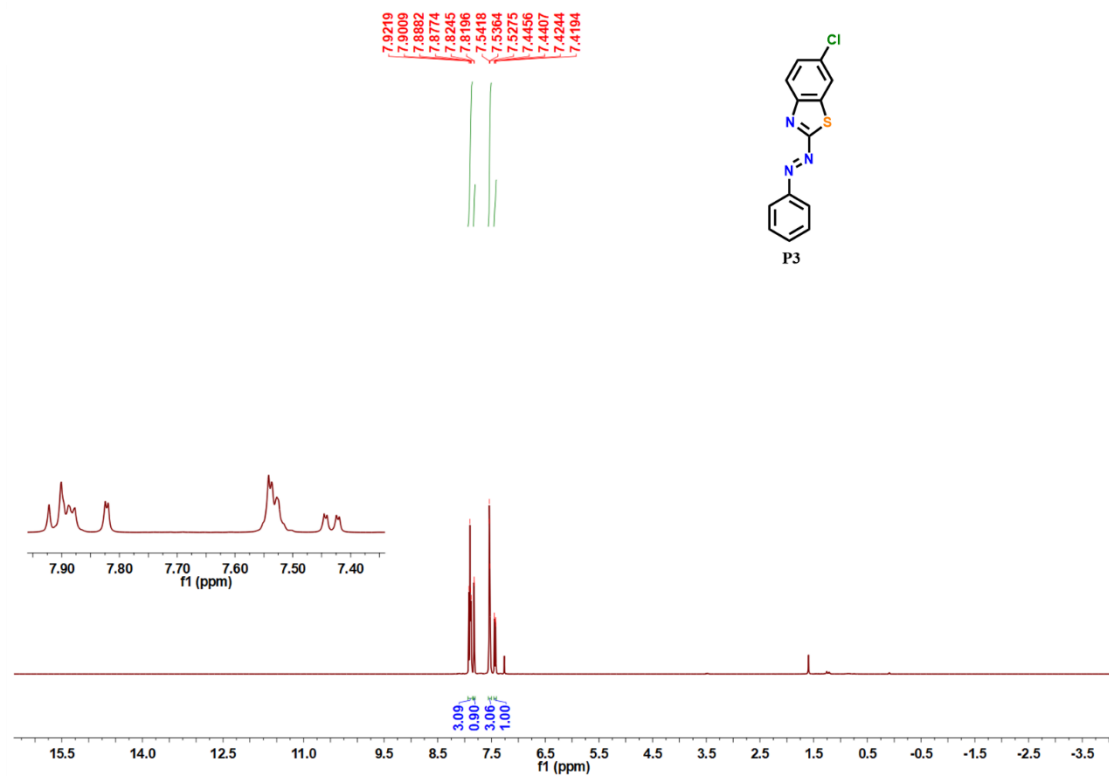


Figure S8.5. ¹H (400 MHz) NMR spectrum of P3 in CDCl₃.

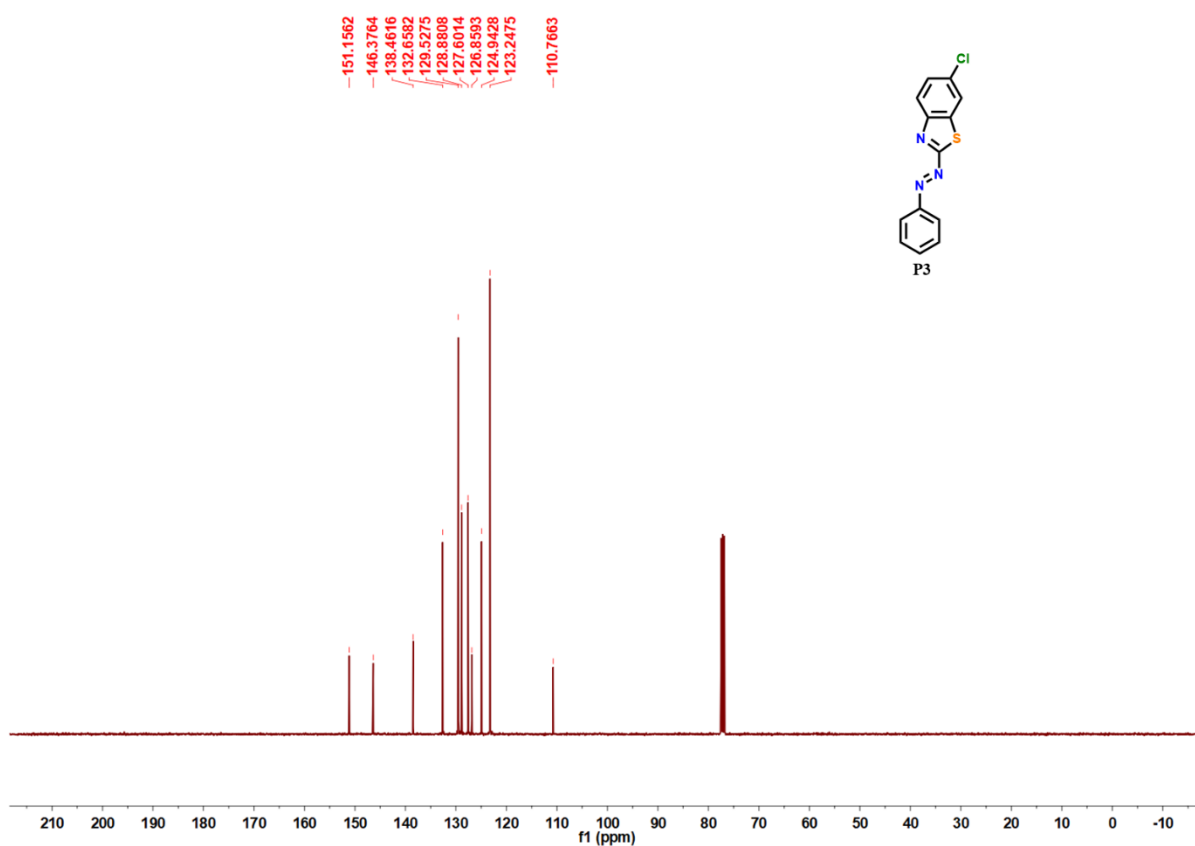


Figure S8.6. ¹³C (100 MHz) NMR spectrum of P3 in CDCl₃.

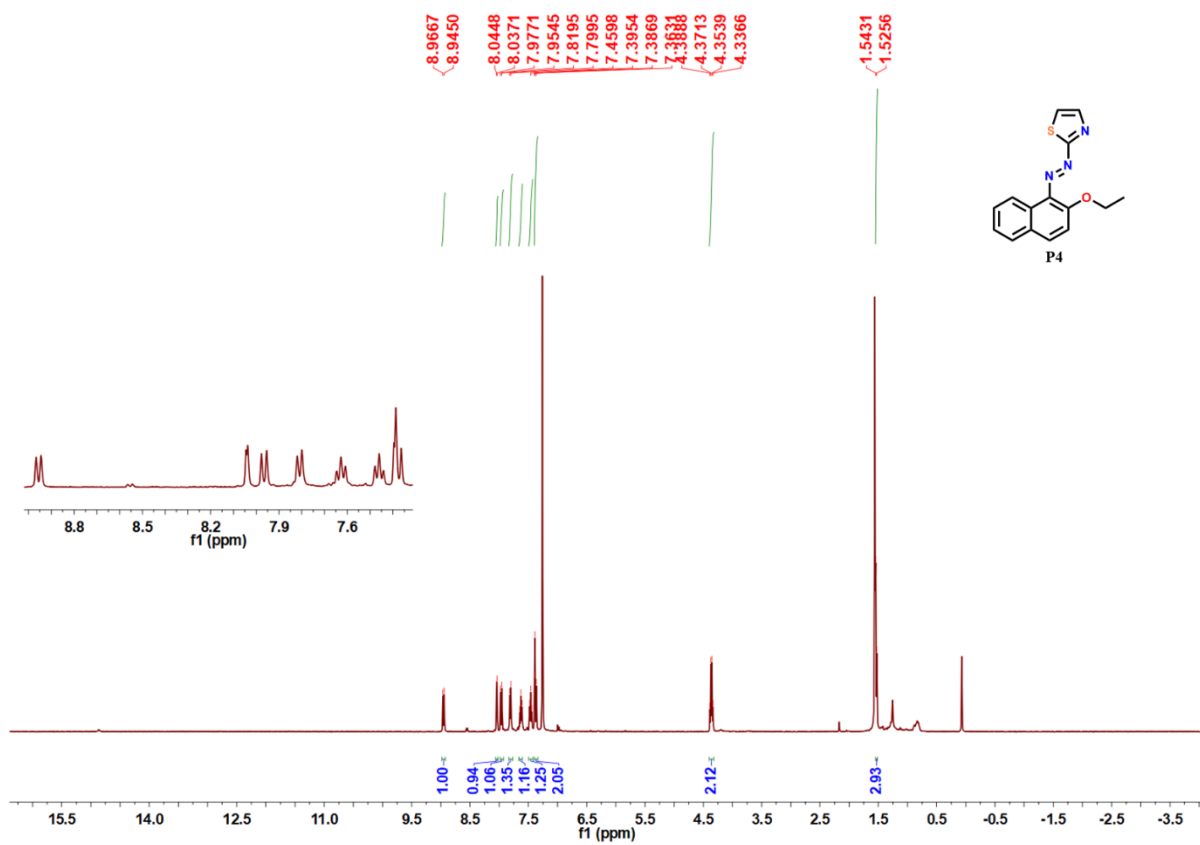


Figure S8.7. ¹H (400 MHz) NMR spectrum of P4 in CDCl₃.

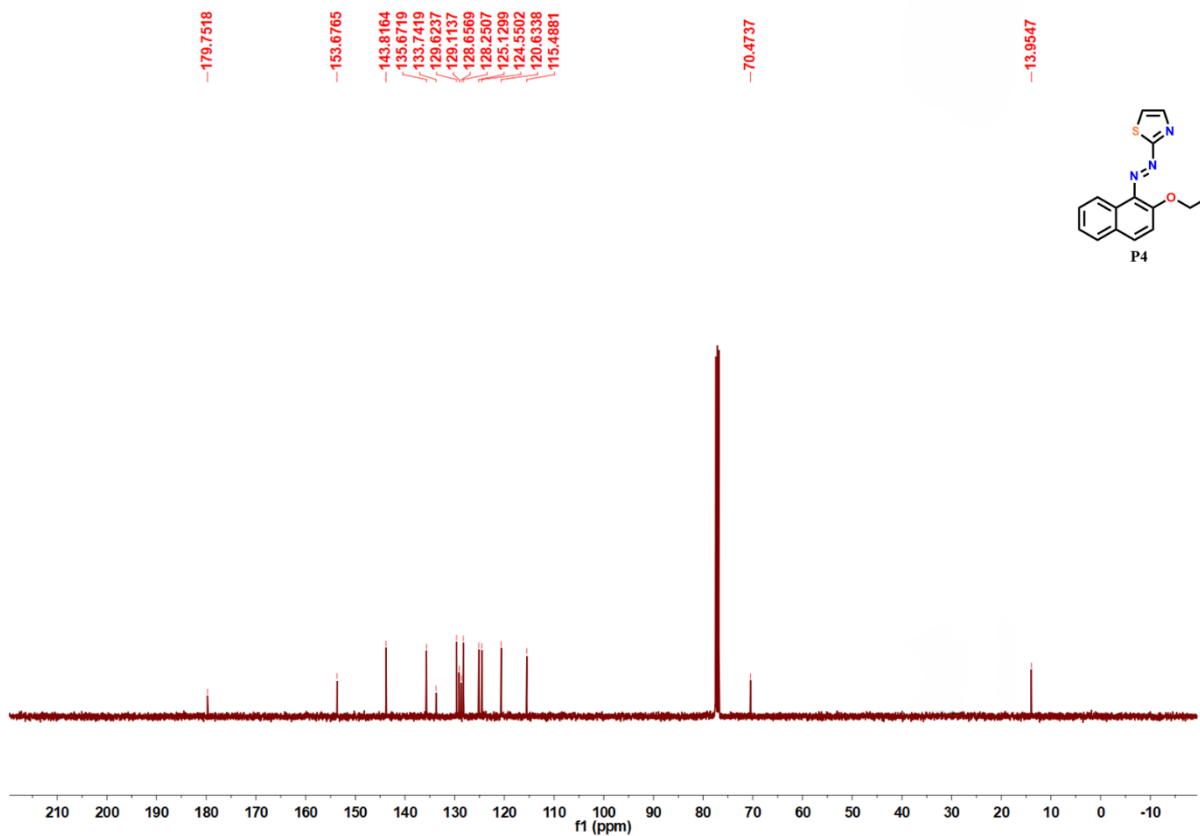


Figure S8.8. ¹³C (100 MHz) NMR spectrum of P4 in CDCl₃.

S9. Other supporting information



Figure S9.1. Images depicting the change in color of **P1** during urea hydrolysis process at different time intervals. (The corresponding movie file Movie M1.mp4 at 5X speed is available as a separate supporting information).

S10. References

- (1) J. S. Renny, L. L. Tomasevich, E. H. Tallmadge and D. B. Collum, *Angew. Chem., Int. Ed., Engl.*, 2013, **46**, 11998-2013.
- (2) H. A. Benesi and J. H. Hildebrand, *J. Am. Chem. Soc.*, 1949, **71**, 2703 -2707.
- (3) M. J. Frisch, G. W. Trucks, H. B. Schlegel, G. E. Scuseria, M. A. Robb, J. R. Cheeseman, G. Scalmani, V. Barone, G. A. Petersson, H. Nakatsuji, X. Li, M. Caricato, A. Marenich, J. Bloino, B. G. Janesko, R. Gomperts, B. Mennucci, H. P. Hratchian, J. V. Ortiz, A. F. Izmaylov, J. L. Sonnenberg, D. Williams-Young, F. Ding, F. Lipparini, F. Egidi, J. Goings, B. Peng, A. Petrone, T. Henderson, D. Ranasinghe, V. G. Zakrzewski, J. Gao, N. Rega, G. Zheng, W. Liang, M. Hada, M. Ehara, K. Toyota, R. Fukuda, J. Hasegawa, M. Ishida, T. Nakajima, Y. Honda, O. Kitao, H. Nakai, T. Vreven, K. Throssell, J. A. Montgomery, Jr., J. E. Peralta, F. Ogliaro, M. Bearpark, J. J. Heyd, E. Brothers, K. N. Kudin, V. N. Staroverov, T. Keith, R. Kobayashi, J. Normand, K. Raghavachari, A. Rendell, J. C. Burant, S. S. Iyengar, J. Tomasi, M. Cossi, J. M. Millam, M. Klene, C. Adamo, R. Cammi, J. W. Ochterski, R. L. Martin, K. Morokuma, O. Farkas, J. B. Foresman, and D. J. Fox, *Gaussian 16 Rev. C.01*; Wallingford, CT, 2016.
- (4) A. D. Becke, *J. Chem. Phys.*, 1993, **98**, 5648-5652.
- (5) C. Lee, W. Yang and R. G. Parr, *Phys. Rev. B* 1988, **37**, 785-789.
- (6) S. Grimme, *J. Comput. Chem.* 2004, **25**, 1463-1473.
- (7) R. Krishnan, J. S. Binkley, R. Seeger and J. A. Pople, *J. Chem. Phys.* 1980, **72**, 650-654.
- (8) B. Mennucci, E. Cancès and J. Tomasi, *J. Phys. Chem. B* 1997, **101**, 10506-10517.
- (9) R. F. W. Bader, *Atoms in Molecules: A Quantum Theory*; Clarendon Press, 1994.
- (10) E. R. Johnson, S. Keinan, P. Mori-Sánchez, J. Contreras-García, A. J. Cohen and W. Yang, *J Am. Chem. Soc.* 2010, **132**, 6498-6506.
- (11) T. Lu, and F.Chen, *J. Comput. Chem.* 2012, **33**, 580-592.
- (12) W. Humphrey, A. Dalke and K. Schulten, *J. Mol. Graph.* 1996, **14**, 33-38.